Universitatea Politehnica din Bucuresti
Spl. Independentei 313
060042 Bucuresti
Romania

www.upb.ro

Facultatea de Inginerie Aerospatiala
str. Gh. Polizu 1-5
tel. +40 21 402 3812

www.aero.pub.ro
inginerie.aerospatiala@upb.ro

Department of Aerospace Sciences "Elie Carafoli"

Master program

Air Transport Engineering

Laminar Boundary Layer and Active Control of Fluid Flow

Dissertation

Author: **Sandra Valero Paredes**

Supervisor: **Prof. dr. ing. Dănăilă Sterian**

Date: 27th of June

BUCHAREST

2018

CONTENTS

1 Introduction 6
2 Concept of Boundary Layer 6
2.1 Hypothesis 7
2.2 Boundary Layer Equations 8
2.2.1 Initial and boundary conditions 9
2.3 Karman equation 11
3 Plate Boundary Layer problem 15
3.1 Plate Boundary Layer Equations 15
3.2 Plate Boundary Layer Conditions 16
3.3 Blasius Equation 16
3.4 Blasius Equation Resolution with Numerical Methods 18
3.4.1 Runge-Kutta 4th order method 19
3.4.2 Matlab Code 19
3.4.3 Results 21
4 Control of the Boundary Layer 23
4.1 Controlling Transition by Shaping the Airfoil 24
4.2 Motion of the solid wall 25
4.3 Controlling Transition by Suction 25
4.4 Controlling Separation by Suction 26
4.5 Slit Suction 26
4.6 Tangencial blowing and suction. 27
4.7 Continuous suction and blowing 27
5 Boundary Layer Problem with Fortran Code 28
5.1 Code Description 28
5.1.1 HS Panel Method 28
5.1.2 Printerface code 32
5.1.3 BLP2D code 32
5.2 1st Case: The Influence of the vw 36

5.3 2nd Case: Study of the Optimum Section 36
5.4 3rd Case: Value of $\boldsymbol{vw}$ 36
5.5 4th Case: Influence of the Turbulence 36
6 Numerical results 37
6.1 Suction $\boldsymbol{vw < 0}$ 37
6.1.1 η vs u 37
6.1.2 Cf vs x 38
6.1.3 δ^* vs x 39
6.1.4 θ vs x 40
6.2 Optimum section 41
6.3 Value of $\boldsymbol{vw}$ 43
6.4 Turbulent Flow and Blowing Effect 45
6.4.1 Cf vs x 46
6.4.2 δ^* vs x 47
6.4.3 θ vs x 48
7 Conclusions 49
8 References 49

List of Figures:

Figure 2-1. Development in an airfoil of the boundary layer 6
Figure 2-2. Boundary layer flow along the body surface....7
Figure 2-3. Calculation domain of the boundary-layer equations for external flow. 9
Figure 2-4. Boundary conditions for shear layers. (a) Boundary layer and wake of airfoil. (b) Mixing layer between parallel streams. (c) Merging mixing layer in jet. (d) Merging boundary-layers in internal flow. 10
Figure 2-5. Boundary layer coordinates....11
Figure 3-1. Boundary layer on a zero-incidence flat plate....15
Figure 3-2. Code for Blasius equation (1)....19
Figure 3-3. Code for Blasius equation (2)....20
Figure 3-4. Code for Blasius equation (3)....20
Figure 3-5. Values of f'(η) vs values of k 21
Figure 3-6. Values of f'(η) vs values of η 22
Figure 3-7. Solution of Blasius equation (1908) 22
Figure 4-1. Smoke flow past airfoil at zero angle of attack. 23
Figure 4-2. Same airfoil at large angle of attack with flow separation. 23
Figure 4-3. High-speed photograh of boundary layer on airfoil undergoing transition. Large eddies are formed prior to breakdown into turbulence. 24
Figure 4-4. Rotating circular cylinder inside a fluid flow 25
Figure 4-5. Profile with suction slots on upper surface (indicated by arrowheads). (a) Suction off. Boundary layer is turbulent over most of upper surface. (b) Suction on. Laminar flow restored to upper surface. 25
Figure 4-6. Multi-slotted profile of Figure 4-5 at high angle of attack. (a) Suction on. Separation is prevented. (b) No suction. Flow totally separates from the upper surfaces. 26
Figure 4-7. Circular cylinder with a slit suction inside a fluid flow....26
Figure 4-8. Tangencial blowing inside an airfoil....27
Figure 5-1. NACA Profile Coordinates. 28
Figure 5-2. Panel representation of airfoil surface and notation for an airfoil incidence α 29
Figure 6-1. Representation of *η – u* for station 112. 37
Figure 6-2. Representation of *Cf – x*. 38
Figure 6-3. Comparison of the Displacement Thickness. 39
Figure 6-4. Comparison of the Momentum Thickness. 40
Figure 6-5. Pressure Coefficient of the NACA Profile. 41
Figure 6-6. Comparison for station 112 between two different sections for suction effect. 42
Figure 6-7. Comparison for different values of velocity suction for station 112. 43
Figure 6-8. Comparison of the Ficrtion Coefficient. 44
Figure 6-9. U+ vs Y+ for Blowing. 45
Figure 6-10. Friction coeffficient versus x for turbulent flow. 46
Figure 6-11. Displacement thickness versus x for turbulent flow. 47
Figure 6-12. Theta versus x for turbulent flow. 48

Abstract

The present paper is a theoretical study of the main characteristics of the laminar boundary layer in a fluid flow. It has been researched from the concept of the boundary layer to its importance nowadays. Starting with the Navier-Stokes equations, the boundary layer problem can be simplified through some hypothesis and it is analyzed one of the simplest cases, the plate boundary layer problem, with numerical methods. Furthermore, it has been studied the boundary layer problem through numerical methods with Fortran. It has been studied the types of boundary layer control, active and passive. There cases exposed are for suction and blowing of the boundary layer to compare and show the effects of these types of control.

1 Introduction

The study of the boundary layer theory is one of the main studies in flud dynamics. Since its starts, all the theory and progress has been achieved thanks to all the studies and experiments that lots of scientifics and researchers made this past century. One of the most important developments took place in 1904, [1] when Ludwing Plandtl showed how a theoretical treatment could be used on viscous flows in many practical cases. With some experiments and theoretical considerations, Prandtl showed that the flow past a body can be divided into two regions: a very thin layer close to the body (boundary layer) where the viscosity is important, and the other region outside this layer where the effects of viscosity are not important. This concept helped to understand how important the viscosity is in the drag problem and also it hugely reduced the mathematical difficulty. To support his theory, Prandtl made very simple experiments in a small, self-built water channel, and he also reconnected the theory and practice experiments. Prandtl's frictional layer theory has proved to be extremely useful into the researching field of fluid mechanics. Nowadays, this research still one of the most used in the fluid dynamics field, due to its simplicity and the speed of the calculation. It is common used to solve very difficult problems because it gives a proper estimation to the solving problem.

2 Concept of Boundary Layer

The interest of studying what the boundary layer is and its characteristics is that in many technical applications, fluid flows with low values of viscosity and very high Reynolds numbers are present. At first, it was studied the asymptotic behavior of dimensionless coefficients at high Reynolds numbers, and the boundary-layer theory tries to determine this type of flows behavior at large Reynolds numbers. Frequently, the limiting solution Re = ∞ is a good approximation, but a problem of this solution that the no-slip condition is not satisfied, so the viscosity must be taken into account to satisfy this condition. With the viscosity, velocity transition from the limiting solution's finite value to zero value at the wall. This transition takes place in a thin layer close to the wall at very high Reynolds numbers, which was called by Prandtl as the boundary layer or frictional layer. The boundary layer concept implies that flows with large Reynolds numbers can be divided into two unequally regions. In a certain distance of the wall, viscosity effects are not important, and the viscosity can be neglected. In this first region, the flow corresponds to the inviscid limiting solution, and it is called inviscid outer flow. The second region is located at the wall and corresponds to a very thin boundary layer, where the viscosity must be considered. It is important to mention that within the boundary layer, the two types of flow, laminar and turbulent, can both occur. The following picture explains where the boundary layer is located in an airfoil and also the difference that can be set between the laminar and turbulent flow.

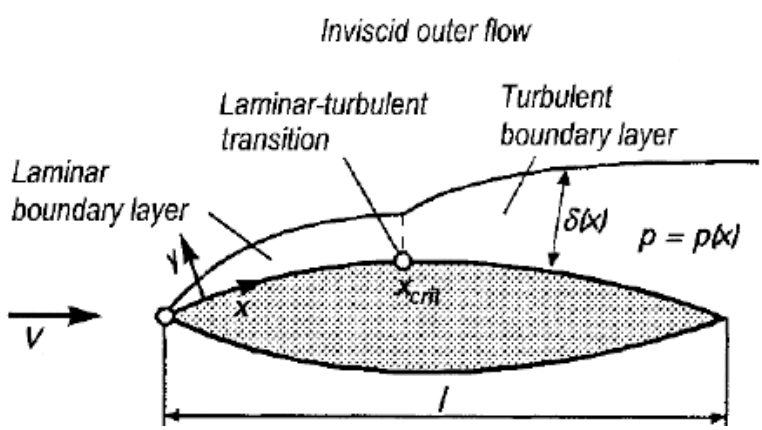

Figure 2-1. Development in an airfoil of the boundary layer

2.1 Hypothesis

In this section, the difference between the flow field into the inviscid outer flow and the boundary layer will be explained, along with the simplifications in the theoretical treatment of flows with high Reynolds numbers. Now, we shall derive the equations from Navier-Stokes for the case of very small friction forces. To simplify, we consider a plane fluid flow with very low viscosity past a slender cilindrical body. The hypothesis are the following:

- Velocities are of the order of V, the magnitude of the free stream velocity, except from the velocities closest to the inmmediate surface of the body.
- Streamline picture and the velocity distribution are almost identical to those of inviscid flow.
- There is a transition from zero at the wall to full velocity, which is located at a certain distance from the wall. This transition takes place in what is called the boundary or frictional layer. Inside this layer we distinguish two zones:
  1. A layer very small along the body where the velocity gradient normal to the wall $\frac{\partial u}{\partial y}$ is very large (boundary layer). In this part, low viscosities μ can be important due to the fact that the viscous shear stress, $\tau = \mu \frac{\partial u}{\partial y}$, can reach significant values.
  2. The other zone outside this layer has no large velocity gradients, so the effects or viscosity can be neglected. The flow in this region is frictionless and potential.

Now, we can assume some simplifications to the problem.

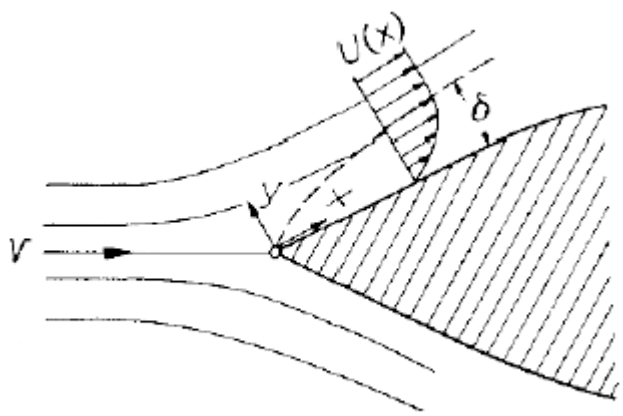

Figure 2-2. Boundary layer flow along the body surface

- First, it will be assumed that the thickness of the boundary layer, δ, as shown in Figure 2-2, is very small compared to a still unspecified linear dimension of the body, l.

$$\delta \ll l \rightarrow \frac{\delta}{l} \ll 1$$

  And the magnitude order of δ is approximately, $\delta \simeq 10^{-2}$.

- Second, the Reynolds number order is approximately, $Re \simeq 10^{4}$.

2.2 Boundary Layer Equations

One of the most important achievements in fluid dynamic was the deduction of the equations for the boundary layer. These were developed with an order of magnitude analysis so that the Navier-Stokes equations of viscous fluid flow can be simplified within the boundary layer. It is appreciated how the characteristic of the partial differential equations becomes parabolic, instead of elliptical as they were in the original form of the full Navier-Stokes equations. This fact greatly simplifies the problem and the equations solution. For solving the problem, the flow is divided into an inviscid portion (outer flow) which can be solved very easily by several methods and with that solution we can resolve the boundary layer region, which should be solved with partial differential equations. Navier-Stokes and continuity equations for a two-dimensional steady incompressible flow in Cartesian coordinates are the following:

$$\frac{\partial u}{\partial x}+\frac{\partial v}{\partial y}=0 \tag{2.1}$$

$$u\frac{\partial u}{\partial x}+v\frac{\partial u}{\partial y}=-\frac{1}{\rho}\frac{\partial p}{\partial x}+\nu\left(\frac{\partial^2 u}{\partial x^2}+\frac{\partial^2 u}{\partial y^2}\right) \tag{2.2}$$

$$u\frac{\partial v}{\partial x}+v\frac{\partial v}{\partial y}=-\frac{1}{\rho}\frac{\partial p}{\partial y}+\nu\left(\frac{\partial^2 v}{\partial x^2}+\frac{\partial^2 v}{\partial y^2}\right) \tag{2.3}$$

In these equations, u and v are the velocity components, ρ is the fluid density, ν is the kinematic viscosity of the fluid at a certain point and p is the pressure.

At the boundary layer, the hypothesis state that, for a large Reynolds number the flow along the surface can be divided into the two regions, where at the boundary layer zone the viscosity effects must be considered. Velocity components, u and v, being now as streamwise and transverse (wall normal) velocities both respectively inside the boundary layer. With scale analysis, the final equations for the boundary layer will be reduce to the following:

$$\frac{\partial u}{\partial x}+\frac{\partial v}{\partial y}=0 \tag{2.4}$$

$$u\frac{\partial u}{\partial x}+v\frac{\partial u}{\partial y}=-\frac{1}{\rho}\frac{\partial p}{\partial x}+\nu\frac{\partial^2 u}{\partial y^2} \tag{2.5}$$

In the outer flow, the equations are given by:

$$U\frac{\partial U}{\partial x}=-\frac{1}{\rho}\frac{\partial p}{\partial x} \tag{2.6}$$

2.2.1 Initial and boundary conditions

The boundary-layer equations are parabolic partial differential equations and are much easier to solve and less costly than the Reynolds averaged Navier-Stokes equations which are elliptic. These equations are also associated with the inviscid flow equations. The approximations used to obtain these, however, are not valid in the same region of the flow. The boundary-layer equations apply close to the surface of a body and in wakes which form behind the body. The inviscid flow equations apply outside the boundary-layer.

For external flow, the behavior of the boundary-layer equations is similar to the behavior of the heat conduction equation. A small perturbation introduced in the boundary-layer diffuses instantaneously along a normal to the wall and is transported downstream along the local streamlines in the boundary-layer. The influence domain of a point P is limited by a line normal to the wall passing through P, by the wall and by the boundary-layer edge. Therefore, if we wish to calculate the boundary-layer in a domain D shown in Figure 2-3, boundary or initial conditions are required along the upstream line normal to the wall, along the and along the outer edge which defines the domain D.

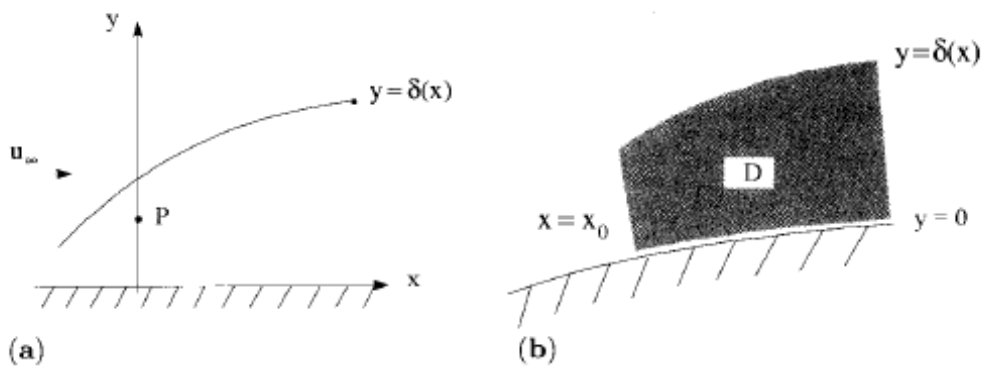

Figure 2-3. Calculation domain of the boundary-layer equations for external flow.

This choice of boundary conditions is justified by the fact that a perturbation introduced along these bounding lines influences the flow in the calculation domain. Along the downstream boundary, no boundary condition is required because a perturbation does not influence the calculation domain, as the velocity u is positive. If u is negative, information can propague upstream. In addition, the two-dimensional steady boundary-layer equations are singular at the point where the wall shear τ_w vanishes. This point is defined as the separation point and the treatment of separated flow region becomes much more involved.

In external flows, the shear layer flowing in the x-direction adjoin an effectively "inviscid" freestream extending to $y = \infty$. On the lower side there may be either a solid surface, usually taken as $y = 0$ as shown in Figure 2-4a, in which case the viscous region is called a "wall shear layer", or there may be another inviscid stream extending to $y = -\infty$ (Figure 2-4b), in which case the viscous region is called a "free shear layer."

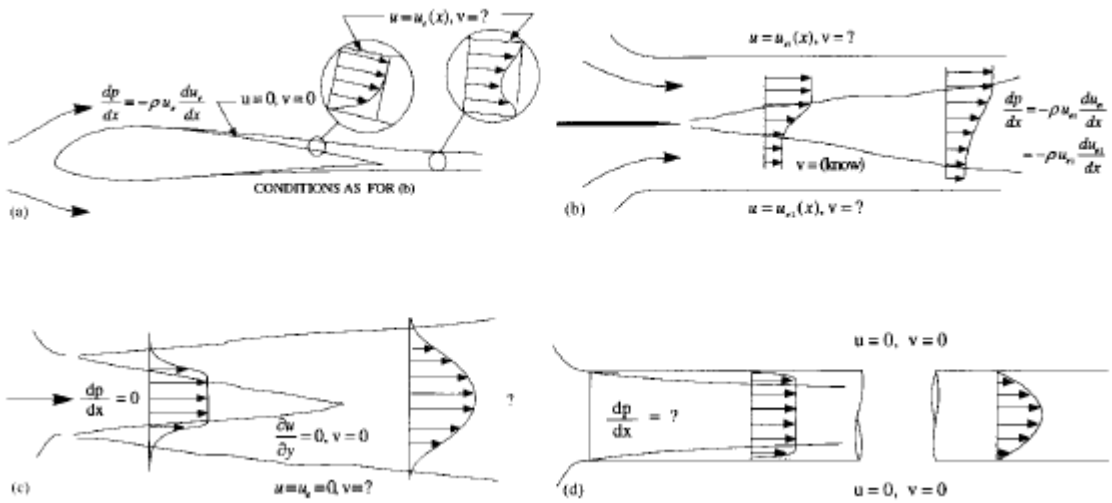

Figure 2-4. Boundary conditions for shear layers. (a) Boundary layer and wake of airfoil. (b) Mixing layer between parallel streams. (c) Merging mixing layer in jet. (d) Merging boundary-layers in internal flow.

In the former case there are three boundary conditions for the velocity field that must be specified, two at the wall, and the other at the boundary-layer edge $y = \delta$. The conditions at the wall involve the specification of normal (v) and tangential (u) components of velocity, and at the edge the specification of the external velocity, that is,

$$y = 0, \quad u = 0, \quad v = v_w(x) \tag{2.7}$$

$$y = \delta, \quad u = u_e(x) \tag{2.8}$$

Here δ is sufficiently large so that dimensionless $\partial u/\partial y$ at the boundary-layer edge is small, say around 10^{-4}. The transpiration velocity, $v_w(x)$, may be either suction or injection. On a nonporous surface it is equal to zero.

In free shear layers (Figure 2-4b and c), the external velocity must be specified in both edges. The difficulties associated with the v boundary condition in free shear layers are less obvious. If the flow is simetrical (Figure 2-4a), no problem arises; the initial symmetrical velocity profiles is specified and v is not required to be zero on the centerline and $u = u_e$ at one edge. If the flow is not symmetrical (Figure 2-4b), a *boundary condition for v cannot be found* from consideration of the shear layer and the boundary layer equations alone. In the real flow the behavior of v outside the shear layer dependes on the v-component equation of motion and the continuity equation, applied throughout the flow and not merely n the shear layer. Of course, a similar problem occurs in determining u_e either in the boundary-layer or wake of Figure 2-4a; the latter problem is both more familiar and mess perplexing.

Internal flows (Figure 2-4d) consist of shear layer of layers filling part or all of the space between two solid boundaries. In this case the pressure distribution is set predominantly by the displacement effect of the shear layer. It is convenient to distinguish flows in which the shear layer fill the cross section and flows such as that near the entrance to a duct (the left-hand part of Figure 2-4d) where a region of effectively inviscid flow obeying Bernoulli's equation remains.

It is also convenient to distinguish the "entrance region", in which the velocities change with x, and the "fully developed" region far downstream in a constant area duct, in which the velocities do not, but of course the pressure continues to decrease with x. The relevant boundary conditions in each case are similar to thos for external flows, except that it is also necessary to satisfy the requirement of constant mass flow between the solid surfaces.

For the boundary layer conditions, the coordinates are assumed to be in the surface of the body, as shows the following picture.

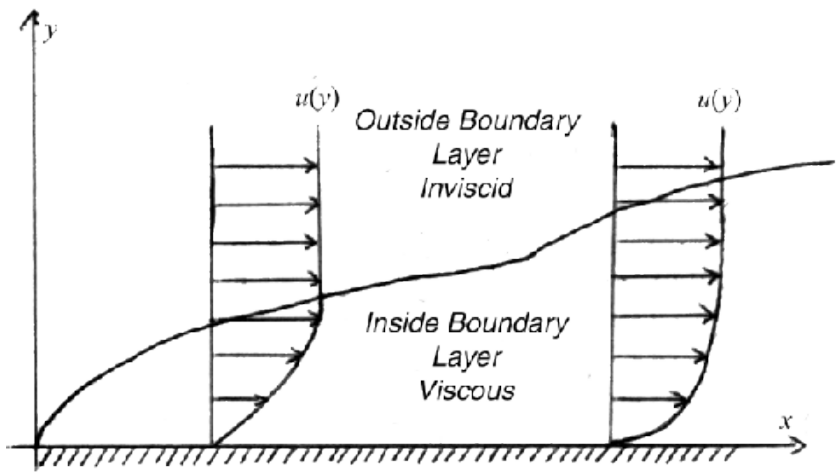

Figure 2-5. Boundary layer coordinates

At the wall, when *y* component is zero, the velocities are zero too due to the non-slip condition. For *y* component is infinite (or δ), the velocity distribution *u* is equal to the velocity in the outer flow, *U(x)*.

$$y = 0 \ \rightarrow u = v = 0 \tag{2.7}$$

$$y = \delta \ \rightarrow u = U(x) \tag{2.8}$$

In the following section, it will be explained the integral form of the boundary layer, known as the Karman equation.

2.3 Karman equation

For solving the boundary layer, it is very useful to solve the integral relation of the boundary layer. In many practical cases, certain integral values of the boundary layer are more interesting than the velocity field. This integral values for the global description of the boundary layer can be calculated using an integration os the boundary layer equations with respect to *y* parameter over the boundary layer thickness.

The problem starts with equations (2.4), (2.5) and (2.6). The conditions are given by (2.7) and (2.8). The first step is to introduce equation (2.6) into (2.5), as follows:

$$u\frac{\partial u}{\partial x} + v\frac{\partial u}{\partial y} = U\frac{\partial U}{\partial x} + \nu\frac{\partial^2 u}{\partial y^2} \tag{2.9}$$

The unknows to solve are *u* and *v*, and we know that there is a certain height, *h*, everywhere outside the boundary layer, $h > \delta$.

The following step is to transform the frist part of (2.9) equation to its conservative form:

$$u\frac{\partial u}{\partial x}+v\frac{\partial u}{\partial y}=\frac{\partial}{\partial x}(u^2)-u\frac{\partial u}{\partial x}+\frac{\partial}{\partial y}(u\cdot v)-u\frac{\partial v}{\partial y} \tag{2.10}$$

Taking into account equation (2.4) is equal to zero, (2.10) can be written as:

$$u\frac{\partial u}{\partial x}+v\frac{\partial u}{\partial y}=\frac{\partial}{\partial x}(u^2)+\frac{\partial}{\partial y}(u\cdot v)-u\cancelto{0}{\left(\frac{\partial u}{\partial x}+\frac{\partial v}{\partial y}\right)} \tag{2.11}$$

Equation (2.11) is replaced in (2.9) as follows:

$$\frac{\partial}{\partial x}(u^2)+\frac{\partial}{\partial y}(u\cdot v)=U\frac{\partial U}{\partial x}+\nu\frac{\partial^2 u}{\partial y^2} \tag{2.12}$$

Now, equation (2.12) is integrated in both sides of the equation, which limits are from zero to *h*.

$$\int_0^h\left(\frac{\partial}{\partial y}(u\cdot v)+\frac{\partial}{\partial x}(u^2)\right)\partial y=\int_0^h\left(U\frac{\partial U}{\partial x}+\nu\frac{\partial^2 u}{\partial y^2}\right)\partial y \tag{2.13}$$

1st intregral

$$\int_0^h\left(\frac{\partial}{\partial y}(u\cdot v)\right)\partial y=u\cdot v|^h-\cancelto{0}{u\cdot v|^0}=u|^h\cdot v|^h=U\cdot v_h \tag{2.14}$$

Velocity components at $y = 0$ are zero due to condition (2.7). Velocity u at $y = h$ it is the external velocity of the flow U, but we need to know the value for v at $y = h$.

$$\int_0^h\left(\frac{\partial u}{\partial x}+\frac{\partial v}{\partial y}\right)\partial y=\int_0^h\left(\frac{\partial u}{\partial x}\right)\partial y+v|_0^h=\int_0^h\left(\frac{\partial u}{\partial x}\right)\partial y+v_h \tag{2.15}$$

$$\int_0^h\left(\frac{\partial u}{\partial x}+\frac{\partial v}{\partial y}\right)\partial y=0\ \rightarrow\ v_h=-\int_0^h\left(\frac{\partial u}{\partial x}\right)\partial y \tag{2.16}$$

Finally, introducing (2.16) into (2.14) is obtained the following solution for the first integral.

$$\int_0^h \left(\frac{\partial}{\partial y}(u \cdot v)\right) \partial y = U \cdot v_h = -U \int_0^h \left(\frac{\partial u}{\partial x}\right) \partial y \tag{2.17}$$

2nd integral

$$\int_0^h \left(\nu \frac{\partial^2 u}{\partial y^2}\right) \partial y = \int_0^h \frac{\partial}{\partial y}\left(\nu \frac{\partial u}{\partial y}\right) \partial y \tag{2.18}$$

For this integral, the shear stress definition is needed.

$$\tau = \mu \frac{\partial u}{\partial y} = \rho \frac{\mu}{\rho} \frac{\partial u}{\partial y} = \rho \cdot \nu \frac{\partial u}{\partial y} \;\rightarrow\; \frac{\tau}{\rho} = \nu \frac{\partial u}{\partial y} \tag{2.19}$$

$$\int_0^h \frac{\partial}{\partial y}\left(\nu \frac{\partial u}{\partial y}\right) \partial y = \int_0^h \frac{\partial}{\partial y}\left(\frac{\tau}{\rho}\right) \partial y = \frac{\cancelto{0}{\tau_h} - \tau_w}{\rho} = -\frac{\tau_w}{\rho} \tag{2.20}$$

The shear stress at a certain height, *h*, is zero because there is no variation with *y* axis in the velocity distribution, *u*. At the end, the value of this integral will be minus the wall shear stress divided by the density.

3rd integral

The integrals that have been already solved are replaced in the main equation (2.13).

$$\int_0^h \left(\frac{\partial}{\partial x}(u^2)\right) \partial y - U \int_0^h \left(\frac{\partial u}{\partial x}\right) \partial y = \int_0^h \left(U \frac{\partial U}{\partial x}\right) \partial y - \frac{\tau_w}{\rho} \tag{2.21}$$

$$\int_0^h \left(\frac{\partial}{\partial x}(u^2) - U\left(\frac{\partial u}{\partial x}\right) - U\left(\frac{\partial U}{\partial x}\right)\right) \partial y = -\frac{\tau_w}{\rho} \tag{2.22}$$

$$\int_0^h \left(\frac{\partial}{\partial x}(u^2) - \frac{\partial}{\partial x}(U \cdot u) + u\left(\frac{\partial U}{\partial x}\right) - U\left(\frac{\partial U}{\partial x}\right)\right) \partial y = -\frac{\tau_w}{\rho} \tag{2.23}$$

Now, we need two definitions to express equation (2.23) to its final form.

- Displacement thickness, δ_1

$$\delta_1 = \delta^* = \frac{1}{U}\int_0^{\delta(\infty)} (U-u)\partial y \tag{2.24}$$

- Momentum thickness, δ_2

$$\delta_2 = \theta = \frac{1}{U^2}\int_0^{\delta(\infty)} u\,(U-u)\partial y \tag{2.25}$$

Finally, replacing these two definitions into equation (2.23), the *momentum-integral equation* for plane, incompressible boundary layers is shown.

$$\int_0^h \left(\frac{\partial}{\partial x}(u^2-(U\cdot u)) + \frac{\partial U}{\partial x}(u-U)\right)\partial y = -\frac{\tau_w}{\rho} \tag{2.26}$$

$$\int_0^h \left(\frac{\partial}{\partial x}(u(u-U) + \frac{\partial U}{\partial x}(u-U)\right)\partial y = -\frac{\tau_w}{\rho} \tag{2.27}$$

$$\frac{\partial}{\partial x}\int_0^h \big((u(u-U)\big)dy + \frac{\partial U}{\partial x}\int_0^h (u-U)\,\partial y = -\frac{\tau_w}{\rho} \tag{2.28}$$

$$-\frac{\partial}{\partial x}(U^2\cdot\theta) - U\cdot\frac{\partial U}{\partial x}\cdot\delta^* = -\frac{\tau_w}{\rho} \tag{2.29}$$

$$\boxed{\frac{\partial}{\partial x}(U^2\cdot\theta) + \delta^*\cdot U\frac{\partial U}{\partial x} = \frac{\tau_w}{\rho}} \tag{2.30}$$

The *momentum-integral equation* is very useful to obtain two different type of results. This equation in this form is valid for both laminar and turbulent boundary layers.

1. If $u(x,y)$ is known, the wall shear stress can be calculated with equation (2.30) with more precision and less error than using the definition of the derivative (2.19).
   Friction coefficient and drag friction can be also obtained.

$$C_f = \frac{\tau_w}{\frac{\rho}{2}U^2} \tag{2.31}$$

$$D_f = \int_0^l \tau_w\,\partial s \tag{2.32}$$

Being l the total length of the body surface.

2. Displacement thickness, momentum thickness and boundary layer thickness can be computed using the momentum-integral equation. These parameters are also related with drag friction and they provide very useful information about the boundary layer. This can be study more accurate with the *Karman-Polhausen method*.

3 Plate Boundary Layer problem

The plate boundary layer is one of the simplest examples of application of the boundary-layer equations, where the flow goes along a very thin flat plate. H. Blasius (1908) treated the boundary-layer equations in his doctoral thesis. The plate starts at $x = 0$, extend parallel to x axis with a semi-infinite length. The steady flow will be treated pararallel to x axis with the free stream velocity, U_∞. Due to the constant velocity of the potencial flow, there is no variation of the pressure along x axis, as shown in the picture.

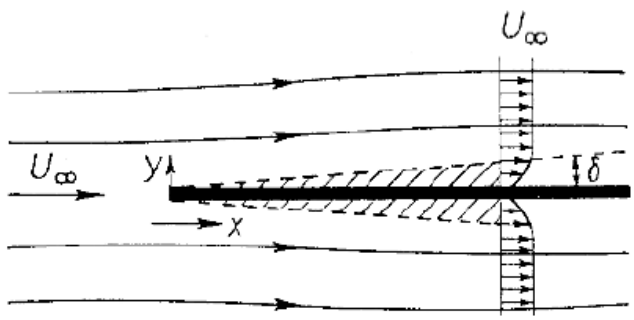

Figure 3-1. Boundary layer on a zero-incidence flat plate

3.1 Plate Boundary Layer Equations

The equations (2.4) and (2.5) can be simplified for this problem with $\frac{\partial p}{\partial x} = 0$

$$\frac{\partial u}{\partial x} + \frac{\partial v}{\partial y} = 0 \tag{3.1}$$

$$u\frac{\partial u}{\partial x} + v\frac{\partial u}{\partial y} = -\frac{1}{\rho}\cancelto{0}{\frac{\partial p}{\partial x}} + \nu\frac{\partial^2 u}{\partial y^2} = \nu\frac{\partial^2 u}{\partial y^2} \tag{3.2}$$

Now, to solve the problem, the stream function, φ, is defined as follows.

$$u = \frac{\partial \varphi}{\partial y} \tag{3.3}$$

$$v = -\frac{\partial \varphi}{\partial x} \tag{3.4}$$

3.2 Plate Boundary Layer Conditions

The conditions that we impose to solve the problem are the following:

$$y = 0 \ \rightarrow u = v = 0 \tag{3.5}$$

$$y = \delta \ \rightarrow u = U_\infty \tag{3.6}$$

The system shown in Figure 3-1 has no characteristic length, so we assume that the velocity distributions at different distances from the leading edge are similar to one another. For *u* velocity profile, we use U_∞ as the scaling factor, while for *y* we use the "boundary layer thickness" *δ(x)*, which increases with *x* distance. Actually, *δ(x)* is not the boundary-layer thickness but a scaled mesure of it which is equal to the boundary-layer thickness up to some numerical factor. We use one similarity law for the velocity profile, where $\varphi(\eta)$ is independent of *x*:

$$\frac{u}{U_\infty} = \varphi(\eta) \tag{3.7}$$

$$\eta = \frac{y}{\delta(x)} \tag{3.8}$$

The resolution of the two partial equations (3.1) and (3.2) are transformed by similarity transformation to lead to an ordinary differential equation for the stream function, called Blasius equation, where all the steps will be explained in the following section.

3.3 Blasius Equation

The first step for the plate boundary-layer resolution is to change equations (3.1) and (3.2) with the stream function definitions (3.3) and (3.4).

$$\frac{\partial}{\partial x}\left(\frac{\partial \varphi}{\partial y}\right) + \frac{\partial}{\partial y}\left(-\frac{\partial \varphi}{\partial x}\right) = 0 \tag{3.9}$$

$$\left(\frac{\partial \varphi}{\partial y}\right) \cdot \frac{\partial}{\partial x}\left(\frac{\partial \varphi}{\partial y}\right) + \left(-\frac{\partial \varphi}{\partial x}\right)\frac{\partial}{\partial y}\left(\frac{\partial \varphi}{\partial y}\right) = \nu \frac{\partial^2}{\partial y^2}\left(\frac{\partial \varphi}{\partial y}\right) \tag{3.10}$$

The conditions change to the following expressions:

$$y = 0 \quad \rightarrow \frac{\partial \varphi}{\partial y} = -\frac{\partial \varphi}{\partial x} = 0 \tag{3.11}$$

$$y = \delta \ \rightarrow \frac{\partial \varphi}{\partial y} = U_\infty \tag{3.12}$$

The similarity variable is defined as follows:

$$\eta \ = y\sqrt{\frac{U_\infty}{\nu\, x}} \tag{3.13}$$

The continuity equation can be integrated introducing a stream function, $\psi(x,y)$.

$$\psi(x,y) = \sqrt{U_\infty \cdot \nu \cdot x} \cdot f(\eta) \tag{3.14}$$

where $f(\eta)$ is the dimensionless stream function.

The next step is to transform the velocity components using the stream function and the similarity variable.

$$u = \frac{\partial \varphi}{\partial y} = \frac{\partial \varphi}{\partial \eta} \cdot \frac{\partial \eta}{\partial y} \tag{3.15}$$

$$v = -\frac{\partial \varphi}{\partial x} = -\left(\frac{\partial \varphi}{\partial x} + \frac{\partial \varphi}{\partial \eta} \cdot \frac{\partial \eta}{\partial x}\right) \tag{3.16}$$

Now, we need to derive the stream function and the similarity variable to obtain the final equation.

$$\frac{\partial \varphi}{\partial \eta} = \sqrt{U_\infty \cdot \nu \cdot x} \cdot f'(\eta) \tag{3.17}$$

$$\frac{\partial \eta}{\partial y} = \sqrt{\frac{U_\infty}{\nu\, x}} \tag{3.18}$$

For *v* velocity distribution we have the following expressions.

$$-\frac{\partial \varphi}{\partial x} = -\frac{\partial}{\partial x}\left(\sqrt{U_\infty \cdot \nu \cdot x} \cdot f(\eta)\right) = -\left(\frac{\partial}{\partial x}\left(\sqrt{U_\infty \cdot \nu \cdot x}\right) \cdot f(\eta) + \sqrt{U_\infty \cdot \nu \cdot x} \cdot \frac{\partial}{\partial x} f(\eta)\right) \tag{3.19}$$

$$\frac{\partial \eta}{\partial x} = -\frac{\eta}{2} \cdot \frac{1}{x} \tag{3.20}$$

$$-\frac{\partial \varphi}{\partial x} = -\sqrt{U_\infty \cdot \nu}\left(\left(\frac{1}{2\sqrt{x}}\right) \cdot f(\eta) + \sqrt{x} \cdot f'(\eta) \cdot \left(-\frac{\eta}{2} \cdot \frac{1}{x}\right)\right) \tag{3.21}$$

All the derivates for the stream function needed for replacing them into equation (3.10) are the following:

$$\frac{\partial \varphi}{\partial y} = U_\infty \cdot f'(\eta) \tag{3.22}$$

$$\frac{\partial^2 \varphi}{\partial y^2} = U_\infty \cdot f''(\eta) \cdot \sqrt{\frac{U_\infty}{\nu\, x}} \tag{3.23}$$

$$\frac{\partial^3 \varphi}{\partial y^3} = \frac{U_\infty^2}{\nu \cdot x} \cdot f'''(\eta) \tag{3.24}$$

$$\frac{\partial \varphi}{\partial x} = \sqrt{U_\infty \cdot \nu}\left(\left(\frac{1}{2\sqrt{x}}\right) \cdot f(\eta) + \sqrt{x} \cdot f'(\eta) \cdot \left(-\frac{\eta}{2} \cdot \frac{1}{x}\right)\right) \tag{3.25}$$

$$\frac{\partial}{\partial x}\left(\frac{\partial \varphi}{\partial y}\right) = \frac{\partial}{\partial x}\left(U_\infty \cdot f'(\eta)\right) = U_\infty \cdot f''(\eta) \cdot \left(-\frac{\eta}{2} \cdot \frac{1}{x}\right) \tag{3.26}$$

Setting all the equation together in equation (3.10) we obtain the Blasius equation.

$$f'''(\eta) + \frac{1}{2} f''(\eta) \cdot f(\eta) = 0 \tag{3.27}$$

3.4 Blasius Equation Resolution with Numerical Methods

Blasius equation is an ordinary differential equation, nonlinear and third order. The three boundary conditions (3.11) and (3.12) are sufficient to determine the solution. This solution can be done by using numerical methods, as Runge-Kutta 4th order method.

Instead of solving the boundary value problem, the initial values at η = 0,

$$f(0) = f'(0) = 0 \tag{3.28}$$

and estimated value,

$$f''(0) = k \tag{3.29}$$

are solved until the following boundary condition is true,

$$f'(\infty) = 1 \tag{3.30}$$

The problem is solved with Matlab®, defining the initial system as follows:

$$f(\eta) = g_1 \tag{3.31}$$
$$f'(\eta) = g_2 \tag{3.32}$$
$$f''(\eta) = g_3 \tag{3.33}$$

Also the derivates are:

$$g_1' = g_2 \tag{3.31}$$
$$g_2' = g_3 \tag{3.32}$$
$$g_3' = -\frac{1}{2} g_1 g_3 \tag{3.33}$$

This last one, (3.33) is obtained using the Blasius equation:

$$g_3' + \frac{1}{2} g_1 \cdot g_3 = 0 \rightarrow g_3' = -\frac{1}{2} g_1 \cdot g_3 \tag{3.34}$$

3.4.1 Runge-Kutta 4th order method

Runge-Kutta method, is an iterative numerical method for solving diferential equations which solves approaching to the solution of an initial value problem. Its expressions for the fourth order method are the following:

$$y' = g' = f(x,y) = B \cdot g^T = \begin{pmatrix} 0 & 1 & 0 \\ 0 & 0 & 1 \\ -\frac{g_3}{2} & 0 & 0 \end{pmatrix} \cdot [g_1\ g_2\ g_3]^T = \left[g_2\ g_3\ \frac{-g_3 g_1}{2}\right]^T \tag{3.35}$$

$$y(x_0) = y_0 \ \rightarrow g_0^T = [0\ 0\ k]^T \tag{3.36}$$

$$y_{i+1} = y_i + \frac{1}{6}h(k_1 + 2k_2 + 2k_3 + k_4) \tag{3.37}$$

The values of the parameters are calculated:

$$k_1 = f(x_i, y_i) = B_i \cdot g_i^T \tag{3.38}$$

$$k_2 = f\left(x_i + \frac{1}{2}h, y_i + \frac{1}{2}k_1 h\right) = B_i \cdot (g_i + \frac{1}{2}k_1 h) \tag{3.39}$$

$$k_3 = f\left(x_i + \frac{1}{2}h, y_i + \frac{1}{2}k_2 h\right) = B_i \cdot (g_i + \frac{1}{2}k_2 h) \tag{3.40}$$

$$k_4 = f(x_i + h, y_i + k_3 h) = B_i \cdot (g_i + k_3 h) \tag{3.41}$$

In this way, the next value y_{i+1} is obtained by the present value y_i plus the product of the interval size, h, multiplied for an estimated gradient. This method of 4th order means that the step error is of the order of $O(h^5)$ while the total error that it has is $O(h^4)$. So that, the convergence of the method is $O(h^4)$ order, that is the reason why it is used in computational methods.

3.4.2 Matlab Code

First, it is defined the values of η, the values of k and the matrix A, that will contain the results. For each iteration of k, we will have a row of values with the numerical method solution for η as columns.

```
clc; clear all;

%%Blasius equation resolution with rk4 %%
eta0=0;
etaf=15;
h=0.05;

N=(etaf-eta0)/h; %temporal step
k0=0.1;
kst=0.01;
kend=1;
kn=100*(kend-k0+kst);
```

Figure 3-2. Code for Blasius equation (1)

The main loop is for each k, with the initial conditions of equation (3.36). The second loop is the Runge-Kutta of 4th order method, where the variables has been explained in the equations from (3.35) to (3.41). The results for $f'(\eta) = g_2$ are saved in A matrix.

```
%Now its defined a matrix with columns as N iteration and rows for each k
A=zeros(kn,N+1);

%The first loop for all k%
for k=k0:kst:kend
    g=[0;0;k]; % Initial conditions for our system

    %The second loop for each k, solving with rk4 the EDO%
    for n=1:N

    B=[0 1 0;0 0 1;(-g(3)/2) 0 0];
    k1=B*g;
    k2=B*(g+0.5*k1*h);
    k3=B*(g+0.5*k2*h);
    k4=B*(g+k3*h);
    g=g+(h/6)*(k1+2*k2+2*k3+k4);

    g2(n+1)=g(2);
    end

    kp=int8(100*(k-k0+kst));

    A(kp,:)=g2;
end
```

Figure 3-3. Code for Blasius equation (2)

This part of the code shows how the final results from the loop are safed into a vector f15 and are plotted with a line where $f'(\eta) = 1$ to obtain the value of k for this result.

```
eta=[eta0:h:etaf];
kvec=[k0:kst:kend];
f15=A(:,N+1);
f15=f15';
y1=ones(1,kn);

figure(1)
plot(kvec,f15,kvec,y1)

%Solution in row 24, k=0.33 and f'(eta)=1%

fsol=A(24,:);
figure(2)
plot(eta,fsol)
```

Figure 3-4. Code for Blasius equation (3)

3.4.3 Results

The results obtained are the two plots that are shown.

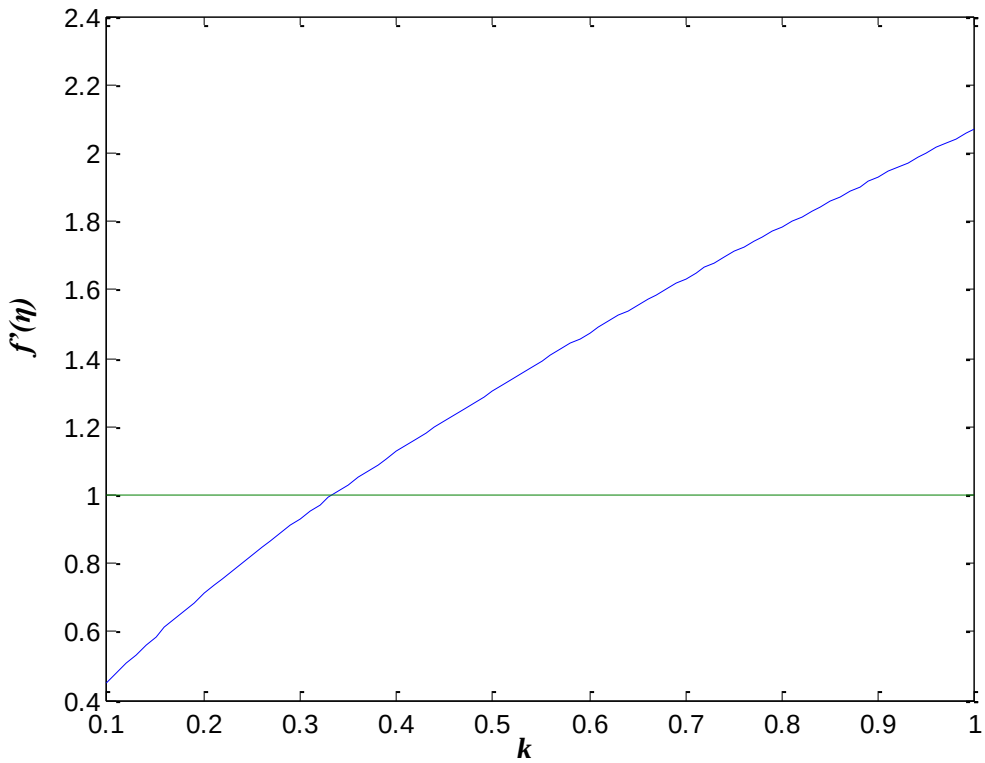

Figure 3-5. Values of f'(η) vs values of k

In the Figure 3-5, the solution to the problem is shown. For the boundary condition $f'(\infty) = 1$, the value of the initial value problem is $k = 0.33$. So that, the next figure will show the distribution of $f'(\eta)$ vs η.

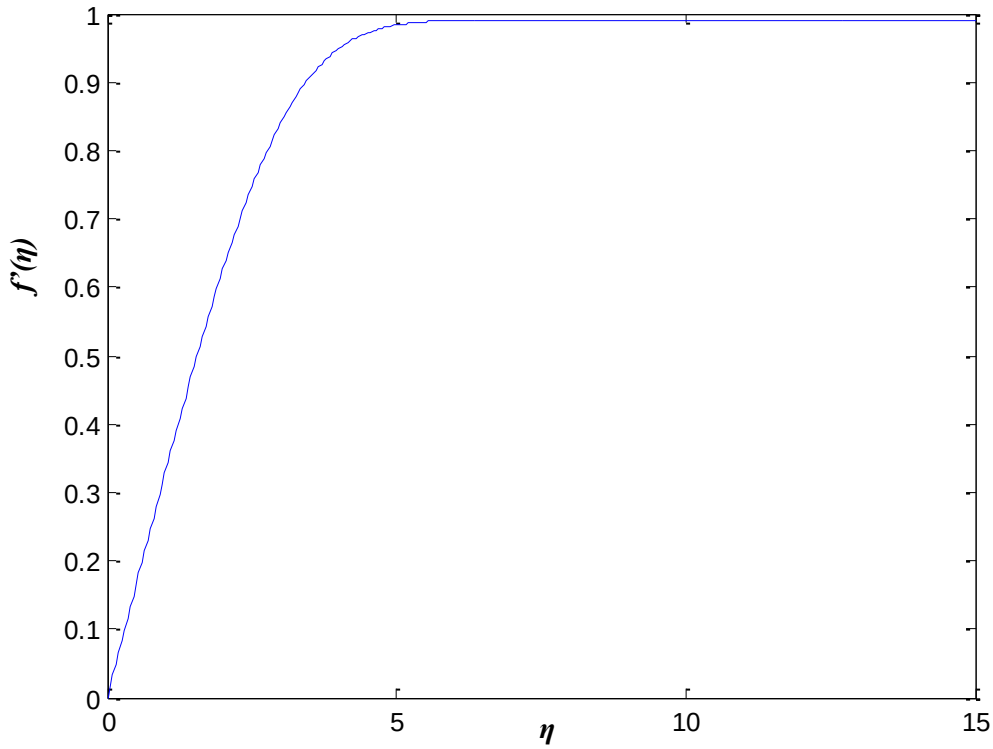

Figure 3-6. Values of f'(η) vs values of η

Finally, the value of $\eta = 5$ is the one that accomplish the boundary condition imposed (3.30). This solution can be compared with the one achieved by Blasius in his doctoral thesis where he obtained the next picture:

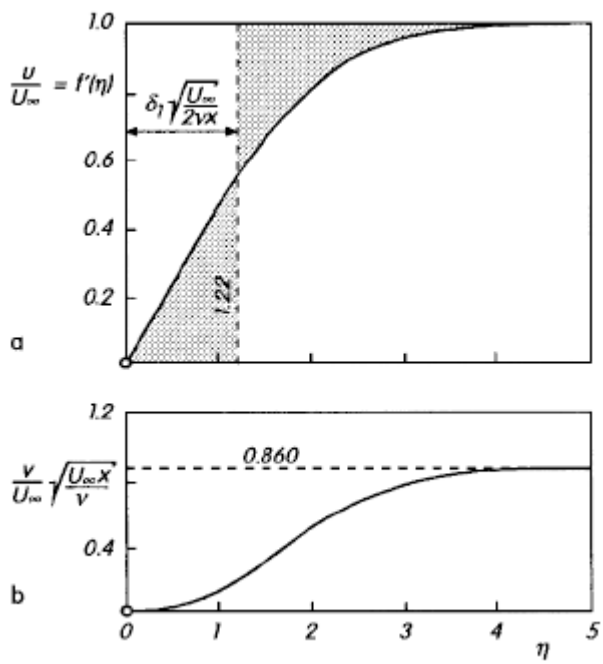

Figure 3-7. Solution of Blasius equation (1908)

4 Control of the Boundary Layer

Potential theory can be used to explain many aerodynamic phenomena, but there are cases in which the boundary layer – the thin layer of fluid next to a solid surface in which effects of viscosity may be considered concentrated – significantly alters theoretical predictions. A simple example is the flow past an airfoil as shown in Figure 4-1, where the airfoil section is in a narrow wind tunnel at zero angle of attack. Kerosene smoke provides the flow visualization [4].

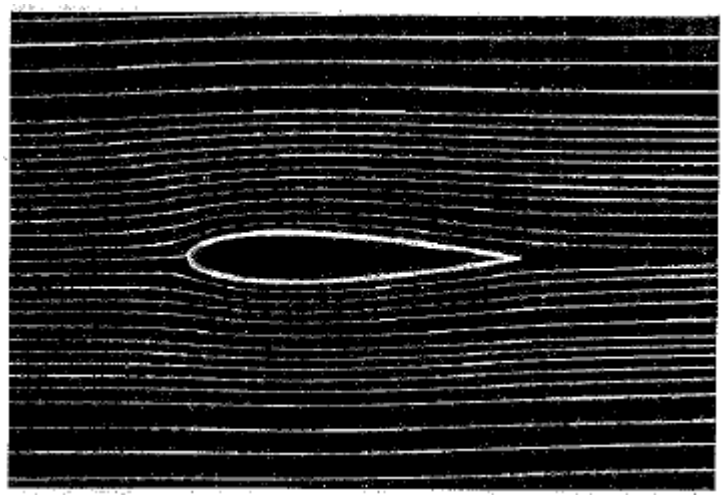

Figure 4-1. Smoke flow past airfoil at zero angle of attack.

At low angles of attack, the streamline pattern about such a shape is very close to the predictions of inviscid theory exists. This drag is largely due to viscous shear forces and is called *skin-friction drag*.

In region over the surface in which the boundary-layer flow is laminar, the fluid mixing and viscous skin friction are low. However, such laminar flows are often unstable and develop into turbulent flows. Turbulent flows involver more rapid mixing, which produces higher skin-friction drag. On occasion, the combined action of viscous forces and an adverse pressure gradient produces a reversal of the flow next to the surface which, in turn, causes separation of the adjacent flow from the surface. This situation is exemplified in Figure 4-2, where the flow on the top surface is separated and the airfoil is said to be stalled.

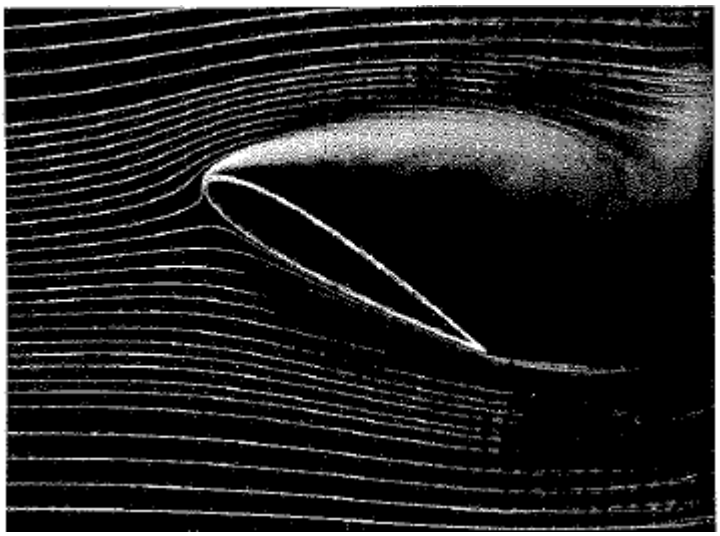

Figure 4-2. Same airfoil at large angle of attack with flow separation.

The presence of the boundary layer has produced many design problems in all areas of fluid mechanics. However, the most intensive investigations have been directed towards its effect upon the lift and drag of wings. The techniques that have been developed to manipulate the boundary layer, either to increase the lift or decrease drag, are classified under the general heading of ***boundary-layer control***.

Two boundary-layer phenomena for which controls have been sought are the transition of a laminar layer to a turbulent flow and the separation of the entire flow from the surface. By maintaining as much of the boundary layer in laminar state as possible, one can reduce the skin friction. By preventing separation, it is possible to increase the lifting effectiveness and reduce the pressure drag. Sometimes the same control can serve both functions.

To sum up, flow control referes to the ability to alter flows with the aim of achieving a desired effect, examples of flow control applications include drag reduction, noise attenuation, improved mixing, or increased combustion efficiency, among many other industrial applications.

A laminar boundary-layer forms when a real (viscous) fluid flow past a solid body. The boundary layer separation represens a major proble which constrains the design of aircraft device. It is characterized by a loss of kinetic energy near solid surface and it depends on the flow regime, which is either laminar or turbulent. Moreover, it is necessary to have a flow separation control. The ways for separation control can be splitted into:

- Passive Control: Vortex generators, Flaps/Slats, Absorbant Surface, Ribles.
- Active Control: Mobile surface, Planform control, Jets, Advanced controls.

Next sections will explain different types of boundary-layer control. The main focuss of this research is active control of the boundary-layer with suction and blowing.

4.1 Controlling Transition by Shaping the Airfoil

Transition to turbulence is associated with instability of the laminar boundary layer. When studied with the aid of high-speed photography, Figure 4-3, disturbances in the laminar flow are seen to amplify to the point of forming large eddies. These in turn produce the highly disorderly motion of turbulent flow. The location on the surface at which transition occurs depends both upon the stability of the laminar boundary layer and upon the nature of the disturbances. Factors producing disturbances, such as surface roughness, noise, vibration, heat, or airstream turbulence, can be sometimes avoided or isolated. The stability of the laminar boundary layer may also be influenced by manipulating the pressure gradient produced by the flow over the surface.

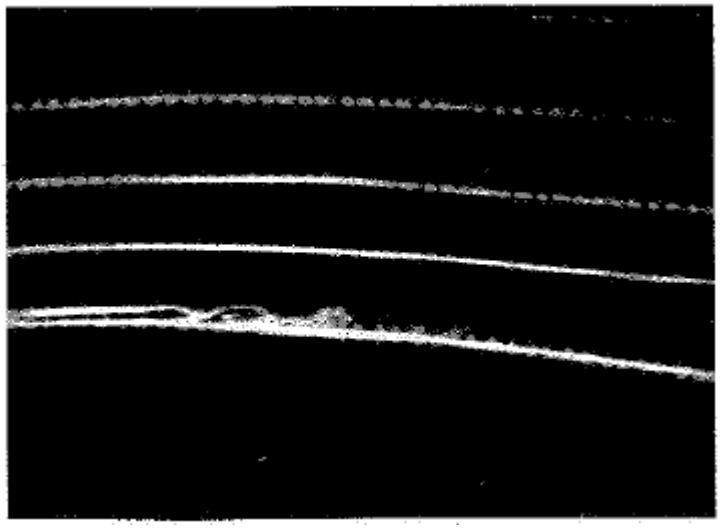

Figure 4-3. High-speed photograh of boundary layer on airfoil undergoing transition. Large eddies are formed prior to breakdown into turbulence.

4.2 Motion of the solid wall

This method completely prevents the formation of a boundary layer. The existence of the boundary layer is due to the velocity difference between the wall and the outer flow, no-slip condition, so boundary layer can be removed if there isn't velocity difference between the wall and the outer flow. Moving the wall along with the flow can achieve this goal.

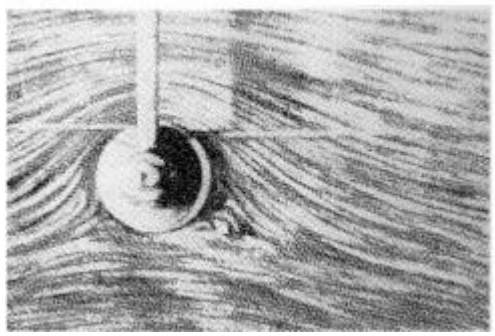

Figure 4-4. Rotating circular cylinder inside a fluid flow

Figure 4-4 describes a perpendicular flow around a rotating circular cylinder where the separation of the boundary layer is completely avoided on the upper side of the cylinder where the direction of the flow and the one in the rotation are the same. In this case the flow field is unsymmetric and the inviscid outer flow corresponds to the cylinder flow with circulation. This flow is producing a transverse force known as the Magnus effect. There has been lots of investigations to apply this type of boundary layer control.

4.3 Controlling Transition by Suction

A rather different means of stabilizing the boundary layer is the use of *suction*. Suction may be applied either through porous surfaces or through a series of finite slots, as in Figure 4-5. When applied in this manner, suction reduces the thickness of the boundary layer by removing the low-momentum fluid next to the surface. A more stable layer results, and transition to turbulence is delayed.

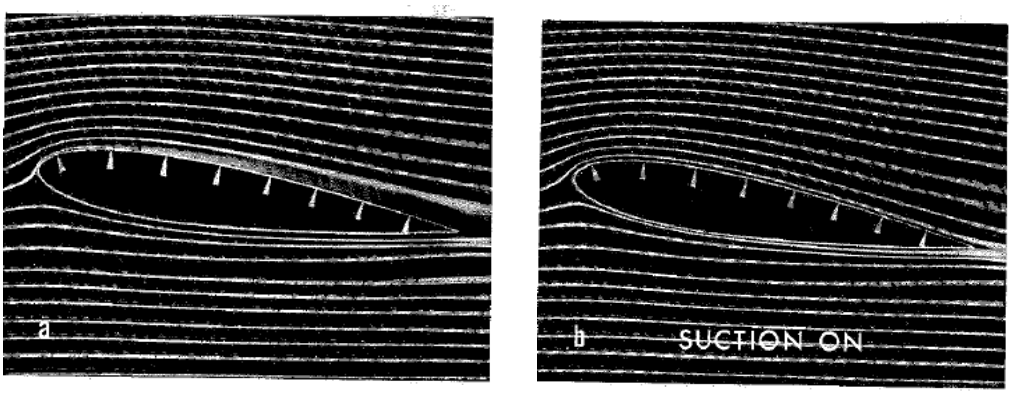

Figure 4-5. Profile with suction slots on upper surface (indicated by arrowheads). (a) Suction off. Boundary layer is turbulent over most of upper surface. (b) Suction on. Laminar flow restored to upper surface.

To achieve stabilization of the boundary layer at various angles of attack, compromises must be made as to the number of slots, their location, and the amount of suction flow through each slot. The application f suction greatly reduces the streamwise momentum loss in the wake. If the suction is applied only in one surface, the wake reduction will not be symmetrical.

Power is needed to achieve this drag reduction. The optimum condition occurs when the total drag – the aerodynamic drag plus the suction power converted to an equivalent drag- is a minimum.

4.4 Controlling Separation by Suction

There are many cases in which control of the boundary-layer separation is important. Suction can be used for this purpose too. If a profile equipped with suction slots is placed at a high enough angle of attack (Figure 4-6 (a)), suction will not be able to maintain the entire boundary ayer in the laminar state. It can, however, exert a profound effect upon the turbulent layer, frequently keeping the flow attached well beyond the angle at which stalling occurs without suction (Figure 4-6 (b)). In general, more suction power is required to attach the flow that is already stalled than to maintain attached flow at the same angle of attack.

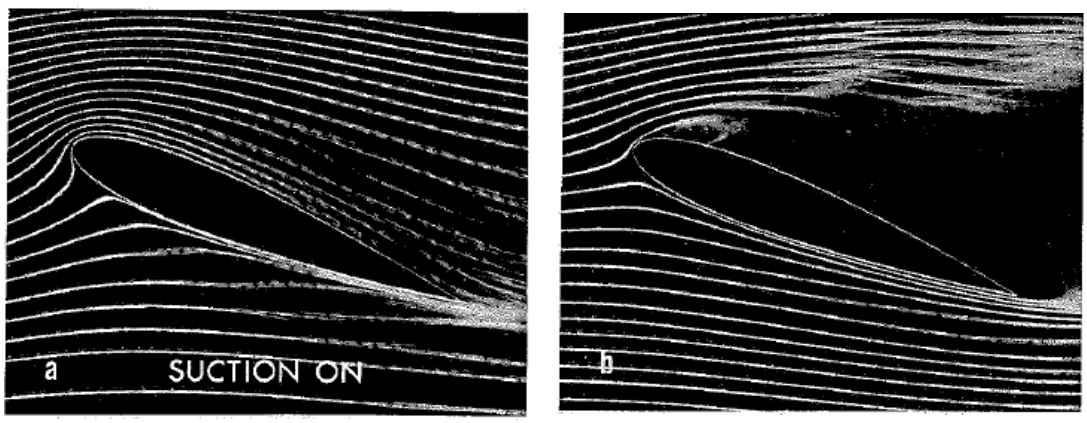

Figure 4-6. Multi-slotted profile of Figure 4-5 at high angle of attack. (a) Suction on. Separation is prevented. (b) No suction. Flow totally separates from the upper surfaces.

Separation control by suction is accomplished by drawing the low-momentum layers from the bottom of the boundary layer intro the suction slots. This draws the higher-energy air from the outer layers closer to the surface.

4.5 Slit Suction

This type of controlling the boundary layer was first studied by Prandtl (1904), he achieved some surprinsing effects. In Figure 4-7 a flow past through a circular cylinder where suction is applied through one side slit.

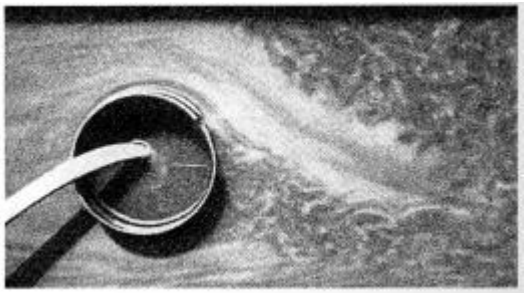

Figure 4-7. Circular cylinder with a slit suction inside a fluid flow

This provoke that the the flow follows along the surface of the body where the suction is applied for a significant distance and preventing separation of the boundary layer. Drag is greatly decreased and simultaneously a transverse force is produced because the flow is unsymmetric.

Slit suction effect is mostly due to the change in the velocity distribution U(x) of the outer flow. The distribution of the inviscid outer flow is superimposed on the velocity distribution of the sink flow coming from the suction slit. This makes the flow accelerates in front of the suction slit preventing the separation. Behind the slit, the sink decelerates the outer flow, but the boundary layer has to star off again from zero thickness and can support now greater adverse pressure gradients without separation.

4.6 Tangencial blowing and suction.

This method is a way of preventing boundary layer separation supplying additional energy to the fluid elements which are low in energy in the boundary layer. This can be achieved by tangencially blowing higher velocity fluid out from inside the body. The separation problem is avoided using the supply of kinetic energy of the boundary layer.

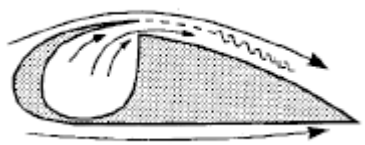

Figure 4-8. Tangencial blowing inside an airfoil

The effectiveness of wing flaps can be greatly improved if there is a fluid tangencially blowing out just in front of the flap (F. Thomas 1962, 1963 - H. Schlichting 1965b). If the intensity of the blown jet is high enough, the lift can be greater than the one predicted by potential theory. The so-called jet flap effect then causes supercirculation (J. Williams 1958). Boundary layer separation can also be prevented by tangential suction, removing the low energy fluid in the boundary layer by suction before it separates. A new boundary layer forms behind the suction slit, and it can achieve a certain pressure increase. If the slit is arranged suitably, in certain circumtances the flow will not separate.

4.7 Continuous suction and blowing

This type of boundary layer control can be achieved if the wall is permeable and let the fluid through. Suction prevents the separation since the low energy fliud in the boundary layer is removed. On the other hand, the wall stress and the friction drag can be reduced by blowing. The most important application of blowing is the transpiration cooling. If a different fluid is injected, a binary boundary layer appears. This boundary layer has velocity and temperature fields as well as a concentration field.

The stability of the boundary layer and the transition to turbulence are also considerably influenced by continuous suction and blowing. Suction always stabilises the boundary layer.

5 Boundary Layer Problem with Fortran Code

In this section, the boundary layer problem will be solved with the code of Cebeci-Cousteix found in the book *Modeling and Computation of Boundary-Layer Flows* [2]. The first case of study is a NACA 4 digits profile and for the second case of study the code will be modified to add suction and blowing to the surface flow around the profile. The airfoil coordinates are shown in Figure 5-1.

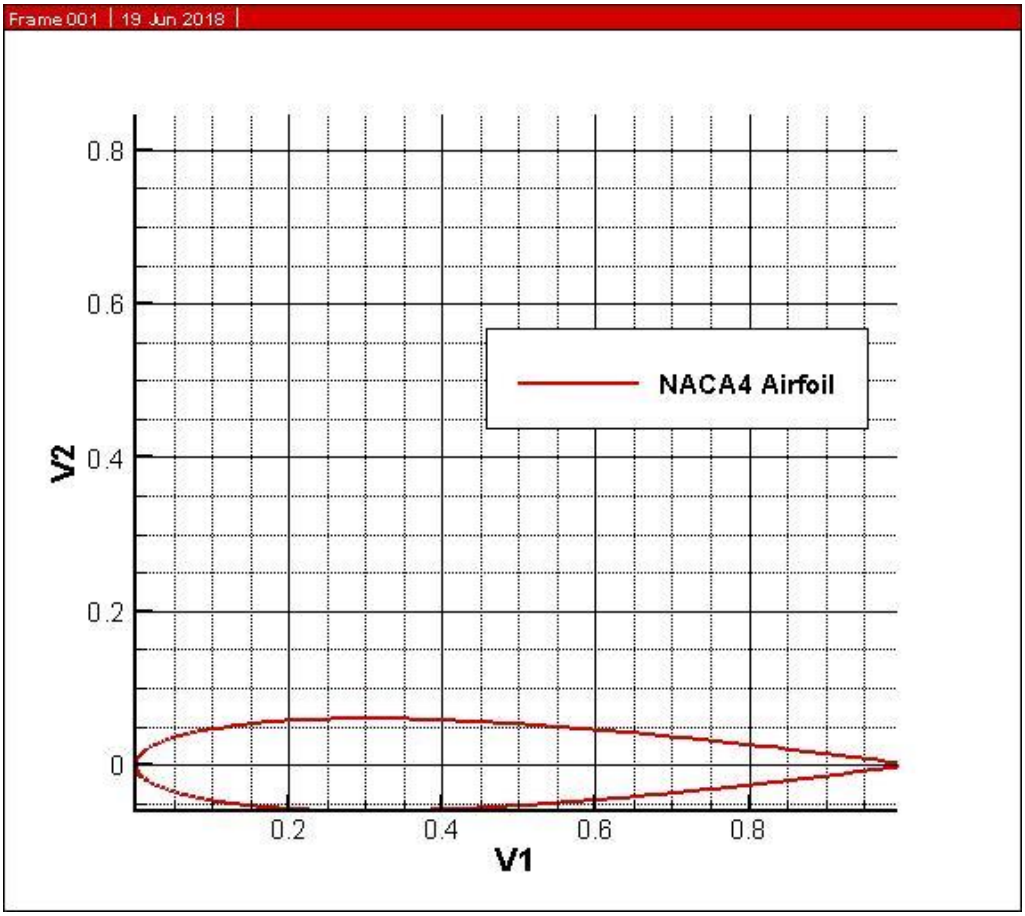

Figure 5-1. NACA Profile Coordinates.

5.1 Code Description

For solving the boundary-layer problem we have four codes connected to each other. First, the external flow is solved with Hess-Smith Panel Method [3]. The next step is to run the data obtained through the printerface code that is made for the user to select the method for solving the problem: Thwaites' method or Boundary-Layer Program for a laminar channel flow. For both cases of the study the second one will be chosen.

5.1.1 HS Panel Method

We consider an airfoil at rest in an onset flow of V_∞. We assume that the airfoil is at an angle of attack, α (the angle between its chord line and the onset velocity), and that the upper and lower surfaces are given by a set of *(x,y)* values of the airfoil coordinates found in *naca4.dat* file. In the following picture it is described the notation used to solve the problem.

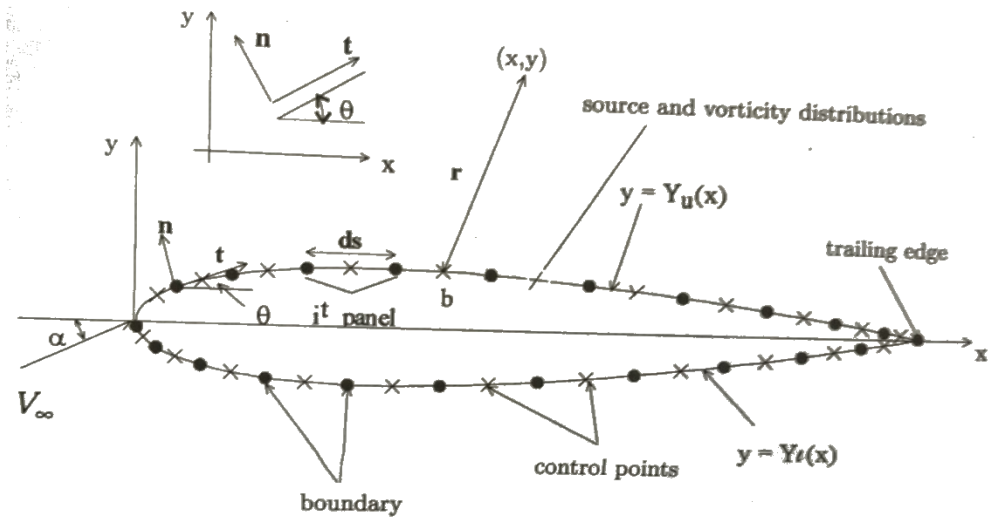

Figure 5-2. Panel representation of airfoil surface and notation for an airfoil incidence α

In the HS panel method, the velocity $\vec{V}$ at any point (x, y) is represented by

$$\vec{V} = \vec{U} + \vec{v} \tag{5.1}$$

Where $\vec{U}$ is the velocity of the uniform flow at infinity:

$$\vec{U} = V_\infty(\cos\alpha\,\vec{\imath} + \sin\alpha\,\vec{\jmath}) \tag{5.2}$$

And $\vec{v}$ is the disturbance field due to the body which is represented by two elementary flows corresponding to source and vortex flows.

A source or vortex on the j-th panel causes and induced source velocity $\vec{v}_s$ at (x, y) or and induced vortex velocity $\vec{v}_v$ at (x, y), respectively, and these are obtained by taking gradients of a potential source

$$\phi_s = \frac{q}{2\pi}\ln r \tag{5.3}$$

And a potential vortex

$$\phi_r = -\frac{I'}{2\pi}\theta \tag{5.4}$$

Both centered at the origin, so we used integrals applied to the airfoil surface,

$$\vec{v}(x,y) = \int \vec{v}_s\, q_j(s)ds_j + \int \vec{v}_v\, \tau_j(s)ds_j \tag{5.5}$$

Each of the N panels is represented by similar sources and vortices distributed on the airfoil surface. The induced velocities in Eq. (5.5) satisfy the irrotationality condition and the boundary condition at infinity.

$$u = \frac{\partial\phi}{\partial x} = \frac{\partial\varphi}{\partial y} = V_\infty\cos\alpha \tag{5.6}$$

$$v = \frac{\partial\phi}{\partial y} = -\frac{\partial\varphi}{\partial x} = V_\infty\, sin\,\alpha \tag{5.7}$$

For uniqueness of the solutions, it is also necessary to specify the magnitude of the circulation around the body. To satisfy the boundary conditions on the body, which correspond to the requirement that the surface of the body is a streamline o the flow, that is,

$$\varphi = constant \quad \text{or} \quad \frac{\partial \phi}{\partial n} = 0 \tag{5.8}$$

At the surface on which *n* is the direction of the normal, the sum of the source-induced and vorticity-induced velocities and freestream velocity is set to zero in the normal direction to the surface of each of the N panels. If the tangential and normal components of the total velocity at the control point of the i-th panel denoted by $(V^t)_i$ and $(V^n)_i$, the flow tangency conditions are then satisfied at panel control points by requiring that the resultant velocity at each control point has only $(V^t)_i$ and

$$(V^n)_i = 0 \quad i = 1,2,\dots,N \tag{5.9}$$

Thus, to solve the Laplace equation with this approach, at the i-th panel control point we compute the normal $(V^n)_i$ and the tangential $(V^t)_i$ velocity components onduced by the source and vorticity distributions on all panels including the i-th itself, and separately sum all the induced velocities for the normal and tangential components together with the freesstream velocity components. The resulting expressions, which satisfy the irrotationality condition, must also satisfy the boundary conditions discussed above. Before discussing this aspect of the problem, it is convenient to write Eq. (5.1) expressed in terms of its velocity components by

$$(V^n)_i = \sum_{j=1}^{N} A_{ij}^n q_j + \sum_{j=1}^{N} B_{ij}^n \tau_j + V_\infty \sin(\alpha - \theta_i) \tag{5.10}$$

$$(V^t)_i = \sum_{j=1}^{N} A_{ij}^t q_j + \sum_{j=1}^{N} B_{ij}^t \tau_j + V_\infty \cos(\alpha - \theta_i) \tag{5.11}$$

Where A_{ij}^n, A_{ij}^t, B_{ij}^n, B_{ij}^t are known as influence coefficients, defined as the velocities induced at a control point (x_{mi}, y_{mi}). More specifically, A_{ij}^n and A_{ij}^t denote the normal and tangential velocity components, respectively, induced at the i-th panel control point by a unit strength source vdistribution on th j-th panel, and B_{ij}^n and B_{ij}^t are those induced by a unit of strength vorticity distribution on th j-th. The influence coefficients are related to eh airfoil geometry and the panel arrangement. The expression that define the matrices are given and calculated in the code in the subroutine COEF (sinalf, cosalf).

For smooth bodies such as ellipse, the problem of rationally determining the circulation has yet to be solved. Such bodies have circulation associated with them, and resulting lift forces, but there is no rule for calculating these forces. If, on the other hand, we deal with an airfoil having a sharp trailing edge, we can apply the Kutta condition. It turns out that for every value of circulation except one, the inviscid velocity is infinite at the trailing edge. The Kutta condition states that the particular value of circulation that gives a finite velocity at the trailing edge is the proper one to choose. This condition does not include bodies with nonsharp trailing edges and bodies on which the viscous effects have been simulated by, for example, surface blowing.

In the panel method, the Kutta condition is indirectly applied by deducing another property of the flow at the trailing edge that is a direct consequence of the finiteness of the velocity. This property is used as the “Kutta condition” and it involve the following:

a. A streamline of the flow leaves the trailing edge along the bisector of the trailing-edge angle.

b. Upper and lower displacement total velocities approach a common limit at the trailing edge. The limiting value is zero if the trailing-edge angle is non-zero.

c. Source and/or vorticity strengths at the trailing edge must satisfy conditions to allow finite velocity.

Of the above, property (b) is more widely used. At first, it may be thought that this property requires setting bth the upper and lower surface velocities equal to zero. This gives two conditions, which cannot be satisfied by adjusting a single parameter. The most reasonable choice is to make these two total velocities in the downstream direction at the 1st and N-th panel control points equal so that the flow leaves the trailing edge smoothly. Since the normal velocity on the surface is zero according to Eq. (5.9), the magnitudes of the two tangential velocities at the trailing edge must be equal, that is,

$$(V^t)_N = -(V^t)_1 \tag{5.12}$$

Introducing the flow tangency condition, Eq. (5.9) into Eq. (5.10) and noting that $\tau_j = \tau$, we get

$$\sum_{j=1}^{N} A_{ij}^n q_j + \tau \sum_{j=1}^{N} B_{ij}^n + V_\infty \sin(\alpha - \theta_i) = 0, \quad i = 1,2,\dots,N \tag{5.13}$$

In terms of the unknows, q_j $(j = 1,2,\dots,N)$ and τ, the Kutta condition of Eq. (5.12) and Eq. (5.13) for a system of algebraic equation which can be written in the following form:

$$A\underline{x} = \underline{b} \tag{5.14}$$

Here, A is a square matrix of order (N+1) and $\vec{x} = (q_1, \dots, q_i, \dots, q_N, \tau)^T$ and $b = (b_1, \dots, b_i, \dots, b_N, b_{N+1})^T$.

First, the elements of a_{ij} are determined by the following equations:

$$a_{ij} = A_{ij}^N, \quad (i,j) = 1,2,\dots,N \tag{5.15}$$

$$a_{i,N+1} = \sum_{j=1}^{N} B_{ij}^n, \quad i = 1,2,\dots,N \tag{5.16}$$

$$a_{N+1,j} = A_{1j}^t + A_{Nj}^t, \quad j = 1,2,\dots,N \tag{5.17}$$

$$a_{N+1,N+1} = \sum_{j=1}^{N} (B_{1j}^t + B_{Nj}^t) \tag{5.18}$$

And the elements of $\vec{b}$ are solved with,

$$b_i = -V_\infty \sin(\alpha - \theta_i), \quad i = 1,2,\dots,N \tag{5.19}$$

$$b_{N-1} = -V_\infty \cos(\alpha - \theta_1) - V_\infty \cos(\alpha - \theta_N) \tag{5.20}$$

So that, the solution of Eq. (5.14) can be obtained by the Gaussian elimination method, which is calculated in the GAUSS (1) subroutine of the *panel.f* code.

Once $\vec{x}$ is determined by GAUSS subroutine so that source strengths q_i $(i = 1,2,\dots,N)$ and vorticity τ on the airfoil surface are known, the tangential velocity component $(V^t)_i$ at each control point can be calculated with VPDIS subroutine. Denoting q_i with $Q(I)$ and τ with GAMMA, the tangential velocities $(V^t)_i$ are obtained with the help of Eq. (5.11). The subroutine also determines the dimensionless pressure coefficient C_P.

To sum up, the code is divided in four main subroutines:

- COEF (SINALF, COSALF): in this subroutine the elements a_{ij} of the matrix A and the elements of $\vec{b}$ are calculated. We note that N+1 corresponds to KUTTA, and N to NODTOT.
- GAUSS (1): the solution of Eq. (5.14) is obtained with the Gauss elimination method.
- VPDIS (SINALF, COSALF): it calculates the tangential velocity component $(V^t)_i$ and the dimensionless pressure coefficient C_P.
- CLCM (SINALF, COSALF): the dimensionless pressure in the appropriate directions is integrated to compute the aerodynamic force and the coefficient for lift (CL) and pitching moment (CM) about the leading edge of the airfoil.

5.1.2 Printerface code

The purpose of this code is to choose the conditions and solver for the boundary-layer problem. It is customary to select the type of flow or the type of method, but for our problem we will choose laminar flow and differential method.

The main parameters and options are the following:

- IFLOW: 0 – for laminar flow, 1 – for laminar and turbulent flow or 2 – for only turbulent flow.
- BIGL: is the reference length that we must choose.
- UREF: is the reference velocity that needs to be selected.
- CNU: is the kinematic viscosity of the flow of study.
- RL: the program calculates the Reynolds' number of the flow.
- Method: 0 – differential (blp2d.f or stp2d.f), 1 – integral (Thwaites' or Head's method).
- IGEOMETRY: this value will provide the program the format of the input data; 0 – panel method or 1 – input [x (I) s (I) Ue (I)].
- Isurface: 0 – lower surface or 1 – upper surface.
- P2: is the dimensionless pressure gradient; 1 – airfoil or 0 – flat plate.

Once all options are chosen, the program calculates points and velocities of the control points for the surface chosen. After this, the distance from the initial point is computed and it generates the input data for the solver.

5.1.3 BLP2D code

This program solves the boundary-layer problem by differential method for two-dimensional flows for obtaining the solutions of the continuity and momentum equations for laminar and turbulent external flows with boundary conditions. BLP2D employs numerical methods for solving the problem and with proper modifications it can also be used for free-shear layer flows and also for internal flows.

In BLP2, the calculation starts at the leading edge, $x = 0$, where the flow is laminar and becomes turbulent at any x-location by specifying the transition location. The program, however, is general and can be modified to include the cases where the calculations start as either laminar or turbulent at a specified x-location.

The solution procedure requires the specification of the dimensionless pressure gradient $m(x)$ and the mass transfer $f_w(x)$ parameters. These two quantities can be obtained from their definitions and the specified reference Reynolds number R_L and the dimensionless external and mass-transfer velocities, $u_e(x)$ and $v_w(x)$ respectively.

The solution procedure also requires the generation of a grid nirmal to the surface, η-grid, and along the surface, x-grid. The latter requirement is usually satisfied by specifying locations with intervals which can be uniform or nonuniform. Its distribution depends on the variation of u_e with x so that the pressure gradient parameter $m(x)$ can be calculated accurately. To ensure this requirement, it is necessary to take small Δx steps (k_n) where there are rapid variations in $u_e(x)$ and where flow approaches separation.

For laminar flows, it is often sufficient to use a uniform grid in the η-direction. For turbulent flows, however, a uniform grid is not satisfactory because the boundary-layer thickness η_e and dimensionless wall shear parameter f_w'' are much larger in turbulent flows than laminar flows. Since short steps in η must be taken to maintain computational accuracy when f_w'' is large, the steps near the wall in a turbulent boundary-layer must be shorter than the corresponding steps in a laminar boundary-layer under similar conditions.

BLP2 consists of a MAIN routine, which contains the logic of computations, and seven subroutines: INPUT, IVPL, GROWTH, EDDY, CMOM, SOLV3 and OUTPUT. The following subsections describe the function of each subroutine except EDDY.

- **MAIN**

BLP2 solves the linearized for of the equations. Through an iterative process, the solution of the equations is obtained for successive estimates of the velocity profiles is needed with subsequent need to check the convergence of the solutions. A convergence criterion based on v_0 which corresponds to f_w'' is usually used and the iterations, which are generally quadratic for laminar flows, are sttoped when

$$\left|\delta v_0\left(= DELV(1)\right)\right| < \epsilon_1 \tag{5.21}$$

With ϵ_1 taken as 10^{-5}. For turbulent flows, due to the approximate linearization procedure used for the turbulent diffusion term, the rate of convergence is not quadratic, and solutions are usually acceptable when the ratio of $|\delta v_0/v_0|$ is less than 0.02. With proper linearization, quadratic convergence of the solutions can be obtained.

After the convergence of the solutions, the OUTPUT subroutine is called and the profiles F, U, V and B, which represent the variables f_j, u_j, v_j and b_j are shifted.

- **Subroutine INPUT**

In this subroutine we generate the η-grid, compute γ_{tr} for the transition region, calculate the pressure gradient parameters m and m_1 and specify η_e at $x = 0$ and the reference Reynolds number R_L.

In addition, the following data are read in and the total number of j-points (NP) is computed.

- **NXT**, total number of x-stations, not to exceed 60.
- **NTR**, NX-station for transition location x_{tr}
- **NPT**, total number of η-grid points
- **DETA(1)**, Δn-initial step size of the variable grid system. Use $\Delta n = 0.01$ for turbulent flows. If desired, it may be changed.
- **ETAE**, transformed boundary-layer thickness, η_e
- **VGP**, K is the variable-grid parameter. Use $K = 1.0$ for laminar flow and $K = 1.14$ for turbulent flow. For a flow consisting of both laminar and turbulent flows, use $K = 1.14$.
- **RL**, Reynolds number
- $\boldsymbol{x}$, surface distance, feet or meters, or dimensionless
- $\boldsymbol{u_e}$, velocity, feet per second or meter per second, or dimensionless

The calculation of m is achieved from the given external velocity distribution $u_e(x)$ and from the definition of m ($\equiv P2$) except for the first NX-station where P2(1) is read in. The derivative of du_e/dx (DUDS) is obtained by using three-point Lagrange interpolation formulas given by ($n < N$):

$$\left(\frac{du_e}{dx}\right)_n = -\frac{u_e^{n-1}}{A_1}(x_{n+1} - x_n) + \frac{u_e^n}{A_2}(x_{n+1} - 2x_n + x_{n-1}) + \frac{u_e^{n+1}}{A_3}(x_n - x_{n-1}) \tag{5.22}$$

Here N refers to the last x^n station and

$$\begin{aligned} A_1 &= (x_n - x_{n-1})(x_{n+1} - x_{n-1}) \\ A_2 &= (x_n - x_{n-1})(x_{n+1} - x_n) \\ A_3 &= (x_{n+1} - x_n)(x_{n+1} - x_{n-1}) \end{aligned} \tag{5.23}$$

The derivative of du_e/dx at the end point $n = N$ is given by

$$\left(\frac{du_e}{dx}\right)_N = -\frac{u_e^{N-2}}{A_1}(x_N - x_{N-1}) + \frac{u_e^{N-1}}{A_2}(x_N - x_{N-2}) + \frac{u_e^N}{A_3}(2x_N - x_{N-2} - x_{N-1}) \tag{5.24}$$

Where now

$$\begin{aligned} A_1 &= (x_{N-1} - x_{N-2})(x_N - x_{N-2}) \\ A_2 &= (x_{N-1} - x_{N-2})(x_N - x_{N-1}) \\ A_3 &= (x_N - x_{N-1})(x_N - x_{N-2}) \end{aligned} \tag{5.25}$$

- **Subroutine IVPL**

Since the equations are solved in linearized from, initial stimates of f_j, u_j and v_j are needed in order to obtain the solutions of the nonlinear Falkner-Skan equation. Various expressions can be used for this purpose. Since Newton's method is used, however, it it useful to provide as good estimate as is possible and an expression of the form.

$$u_j = \frac{3}{2}\frac{\eta_j}{\eta_e} - \frac{1}{2}\left(\frac{\eta_j}{\eta_e}\right)^3 \tag{5.26}$$

Usually satisfies this requirement. The above equation is obtained by assuming a third-order polynomial of the form

$$f' = a + b\eta + c\eta^3 \tag{5.27}$$

And by determining constants a, b, c, from the boundary conditions for the zero-mass transfer case and from one of the properties of momentum equation which requires that $f'' = 0$ at $\eta = \eta_e$.

The other profiles f_j, v_j can be written as

$$f_j = \frac{\eta_e}{4}\left(\frac{\eta_j}{\eta_e}\right)^2\left[3 - \frac{1}{2}\left(\frac{\eta_j}{\eta_e}\right)^2\right] \tag{5.28}$$

$$v_j = \frac{3}{2}\frac{1}{\eta_e}\left[1 - \left(\frac{\eta_j}{\eta_e}\right)^2\right] \tag{5.29}$$

- **Subroutine COEF3**

This is one of the most important subroutines of BLP. It defines the coefficients of the linearized momentum equation.

- **Subroutine SOLV3**

This subroutine uses the block-elimination method determining expressions such as Δ_j, Γ_j, $\vec{w}_j$ and $\vec{\delta}_j$. Noting that the Γ_j matrix has the same structure as B_j and denoting the elements of γ_j, by γ_{ik} $(i, k = 1, 2, 3)$, we can write Γ_j as

$$\Gamma_j \equiv \begin{vmatrix} (\gamma_{11})_j & (\gamma_{12})_j & (\gamma_{13})_j \\ (\gamma_{21})_j & (\gamma_{22})_j & (\gamma_{23})_j \\ 0 & 0 & 0 \end{vmatrix} \tag{5.30}$$

Similarly, if the elements of Δ_j are denoted by α_{ik} we can write Δ_j as

$$\Delta_j \equiv \begin{vmatrix} (\alpha_{11})_j & (\alpha_{12})_j & (\alpha_{13})_j \\ (\alpha_{21})_j & (\alpha_{22})_j & (\alpha_{23})_j \\ 0 & -1 & -\frac{h_{j+1}}{2} \end{vmatrix} \qquad 0 \le j \le J-1 \tag{5.31}$$

And for $j = J$ the elements of the third row, which correspond to the boundary conditions, are $(0, 1, 0)$.

For $j = 0$, $\Delta_0 = A_0$; therefore the values of $(\alpha_{ik})_0$ are

$$\begin{matrix} (\alpha_{11})_0 = 1 & (\alpha_{12})_0 = 0 & (\alpha_{13})_0 = 0 \\ (\alpha_{21})_0 = 0 & (\alpha_{22})_0 = 1 & (\alpha_{23})_0 = 0 \end{matrix} \tag{5.32}$$

All the rest of the parameters are calculated with the expressions given in [3] pages 119 and 120. The subroutine SOLV3 makes use of these formulas to obtain the results.

- **Subroutine OUTPUT**

This subroutine prints out the desired profiles such as f_j, u_j, v_j, and b_j as functions of η_j. It also computes the boundary-layer parameters, c_f, δ^*, θ and R_x. The calculation is made by the trapezoidal rule.

5.2 1st Case: The Influence of the v_w

This study is made to obtain the results of the boundary-layer parameters with the cases of suction and injection. The code was modified to have into account the suction/injection velocity in some stations of the surface profile. The program provides us the pressure gradient in order to choose the correct sequence of stations where the suction or injection velocity will be effective.

The blowing case is going to be studied in the 4th case. For a laminar flow, to blow some fluid in the surface doesn't provide any improvement because the boundary layer separates at the same point of the original airfoil without blowing or suction. For turbulent flows, blowing appears to be effective for the boundary layer because it causes attachement in thr boundary layer at the beginning of it and continues downstream.

5.3 2nd Case: Study of the Optimum Section

In this case, the optimum section for the case of suction is studied. The aim is to obtain the best configuration of the profile with a suction velocity chosen and comparing with other sections. The injection case is rejected due to the results obtained for the 1st case; these results show how suction provide better results and the boundary layer remains more attached rather than with injection.

5.4 3rd Case: Value of v_w

Once we have the results from the other two cases, it is interesting to know which the best value for the suction velocity is, and this value will provide the best results. This is studied through the friction coefficient, because is one of the most important parameters of the boundary layer in an airfoil.

5.5 4th Case: Influence of the Turbulence

For this case, the code was changed to solve with k-epsilon model and to obtain the results for the blowing case. K-epsilon turbulence model is a two-equation model which gives a general description of turbulence by means of two transport equations. The original impetus for the K-epsilon model was to improve the mixing-length model, as well as to find an alternative to algebraically prescribing turbulent length scales in moderate to high complexity flows. The aim is to verify if a small value of blowing in turbulent flow provides a delaying of the separation of the boundary layer.

6 Numerical results

In this section, the results obtained for the four cases explained in 5.2, 5.3, 5.4 and 5.5 are shown and explained to understand the behavior of the boundary layer under the effects of blowing, suction and turbulent flow.

6.1 Suction $v_w < 0$

The boundary layer for the profile chosen is not attached at certain point of the upper surface. So, to include suction will produce a re-attachement in the upper surface of the airfoil for the same angle of attack. The parameters studied are the following.

6.1.1 η vs u

The next figure shows the suction effect compared with the airfoil for the velocity component u versus the adimensional parameter η for station 112 to see how the velocity profile changes over the surface. The following stations are not calculated for the airfoil because the boundary layer is not attached at certain point of the upper surface. The effect starts at station 107 until 180.

- **Station 112**

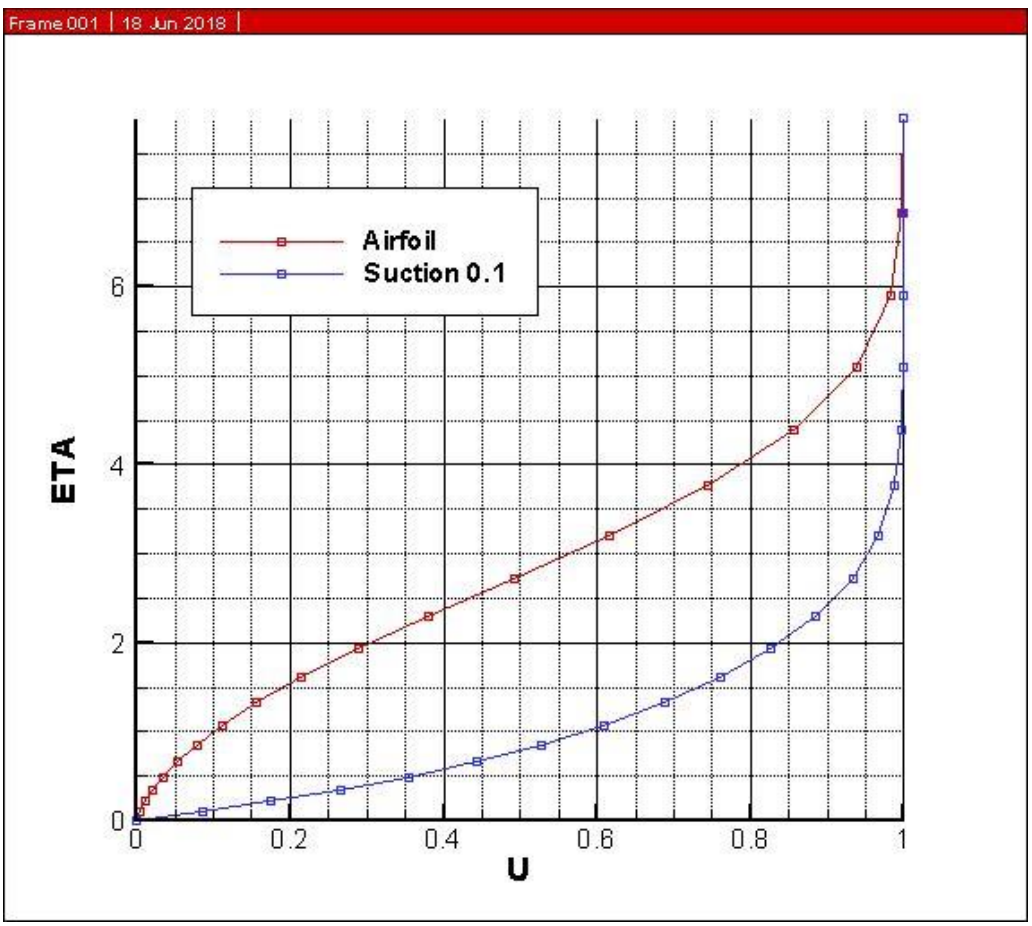

Figure 6-1. Representation of η – u for station 112.

In Figure 6-1 it is shown how at the beginning of the surface, for the station 112 with suction the velocity *u* is greater than the original airfoil without suction. This means that we can achieve a velocity gradient more stable for the firsts station and keep the boundary layer attached from the beginning.

6.1.2 *Cf* vs *x*

Friction coefficient is caused by the viscosity of fluids ad its developed from laminar drag to turbulent drag as fluid moves on the surface. For this case, it is studied to compare the differences between the original airfoil and the suction effect.

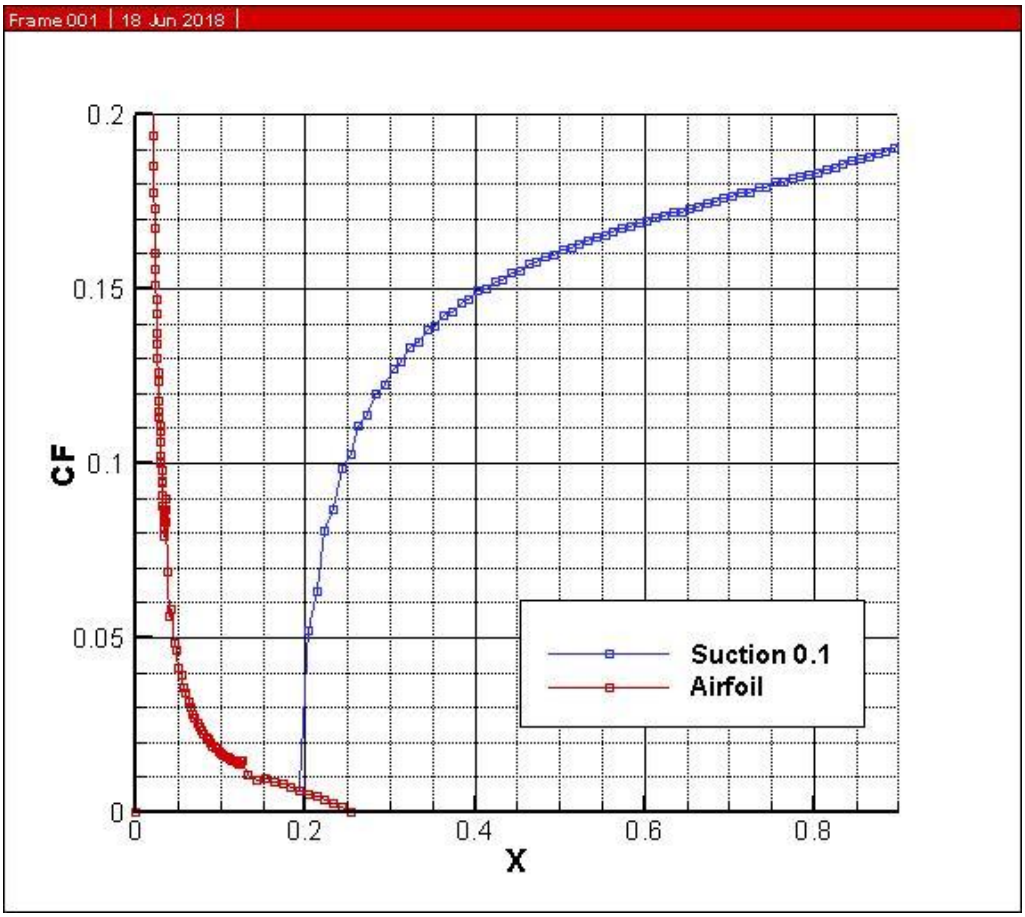

Figure 6-2. Representation of *Cf – x*.

In Figure 6-2 it can be appreciated how for the original airfoil the friction coefficient has smaller values for the beginning of the upper surface of the profile. For the suction case, the values of the friction coefficient are higher due to this effect. It is also important the fact that for the airfoil we only have values until 0.22 approximatly and the value is close to zero. Then the suction effect stars and the friction coefficient increase for the flow downstream.

6.1.3 δ^* vs x

The displacement thickness is the distance by wich a surface would have to be moved in the direction perpendicular to its normal vector away from the reference plane in an inviscid fluid stream of velocity u_0 to give the same flow rate as occurs between the surface and the reference plane in a real fluid. In practical aerodynamics, the displacement thickness essentially modifies the shape of a body immersed in a fluid to allow an inviscid solution. It is commonly used in aerodynamics to overcome the difficulty inherent in the fact that the fluid velocity in the boundary layer approaches asymptotically to the free stream value as disctance from the wall increases at any given location.

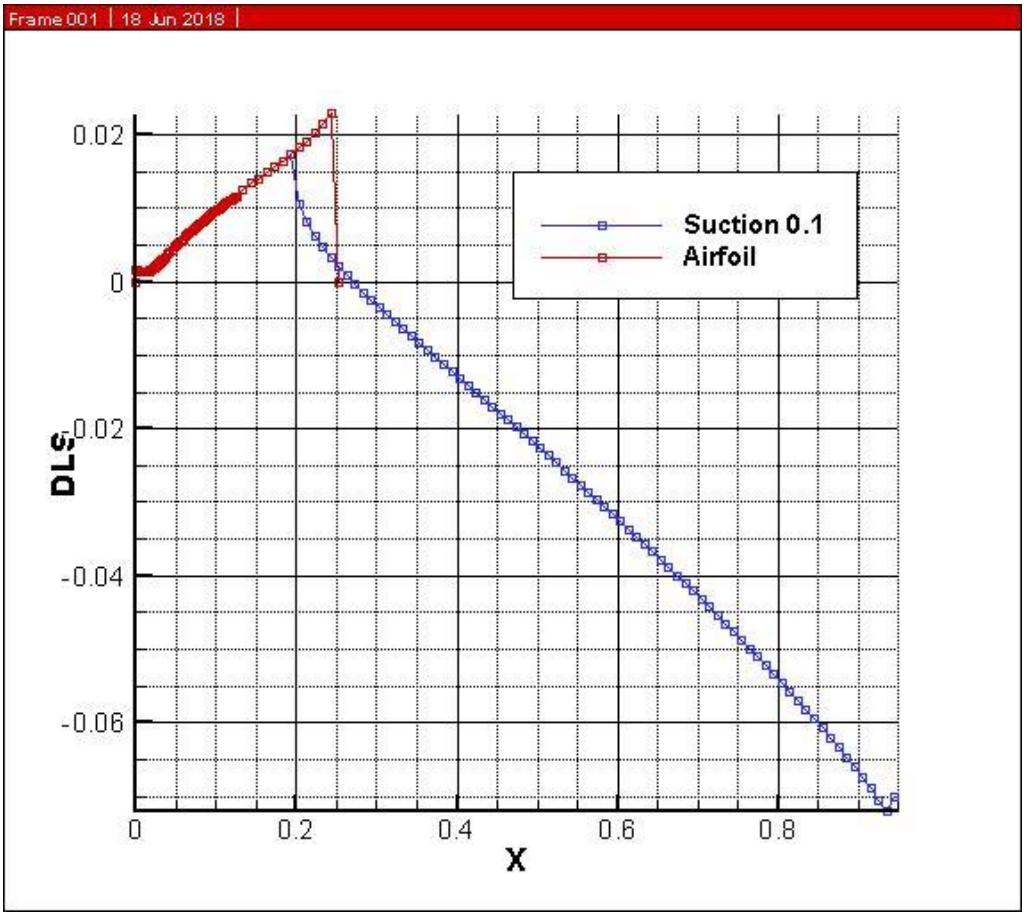

Figure 6-3. Comparison of the Displacement Thickness.

In Figure 6-3, we can see how for the airfoil we only have calculations until the boundary layer separates. For the airfoil including suction, more values are obtained due to the re-attachment of the boundary layer.

6.1.4 θ vs x

The momentum thickness is the distance by which a surface would have to be moved parallel to itself towards the reference plane in an inviscid fluid stream of velocity u_0 to give the same total momentum as exists between the surface and the reference plane in a real fluid.

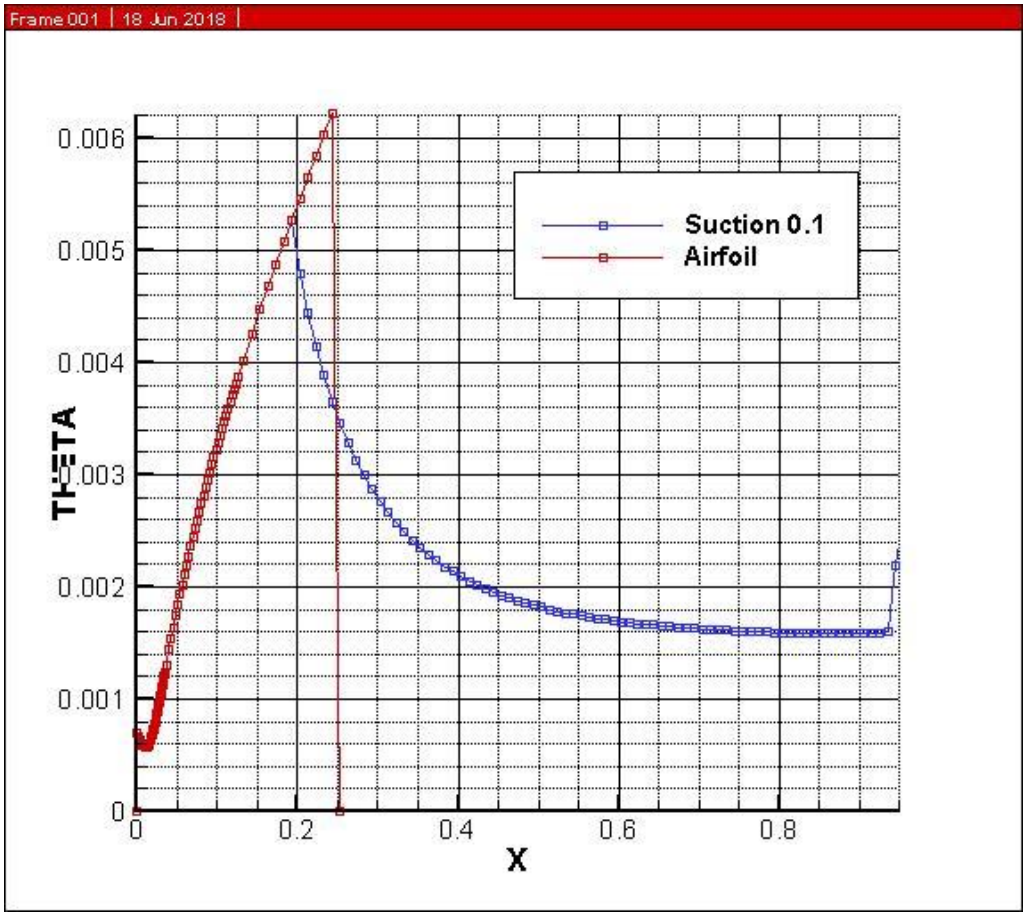

Figure 6-4. Comparison of the Momentum Thickness.

Figure 6-4 shows results that are similar to the other parameters. Due to the suction applied, the boundary layer is attached in the most part of the upper surface of the profile. It is shown how the values of the momentum thickness increase for the airfoil and decreased for the surface where the suction is applied.

6.2 Optimum section

First of all, to study which is the section more effective to locate the suction effect, we should know the pressure coefficient in order to see where we have a greater gradient of pressure to choose the stations for suction. In these stations, the flow will remain attached if we keep this effect and the flow will be laminar in the boundary layer over more sections of the upper surface, delaying the point where the boundary layer starts to separate. This study has different configurations of the sections to choose the better case.

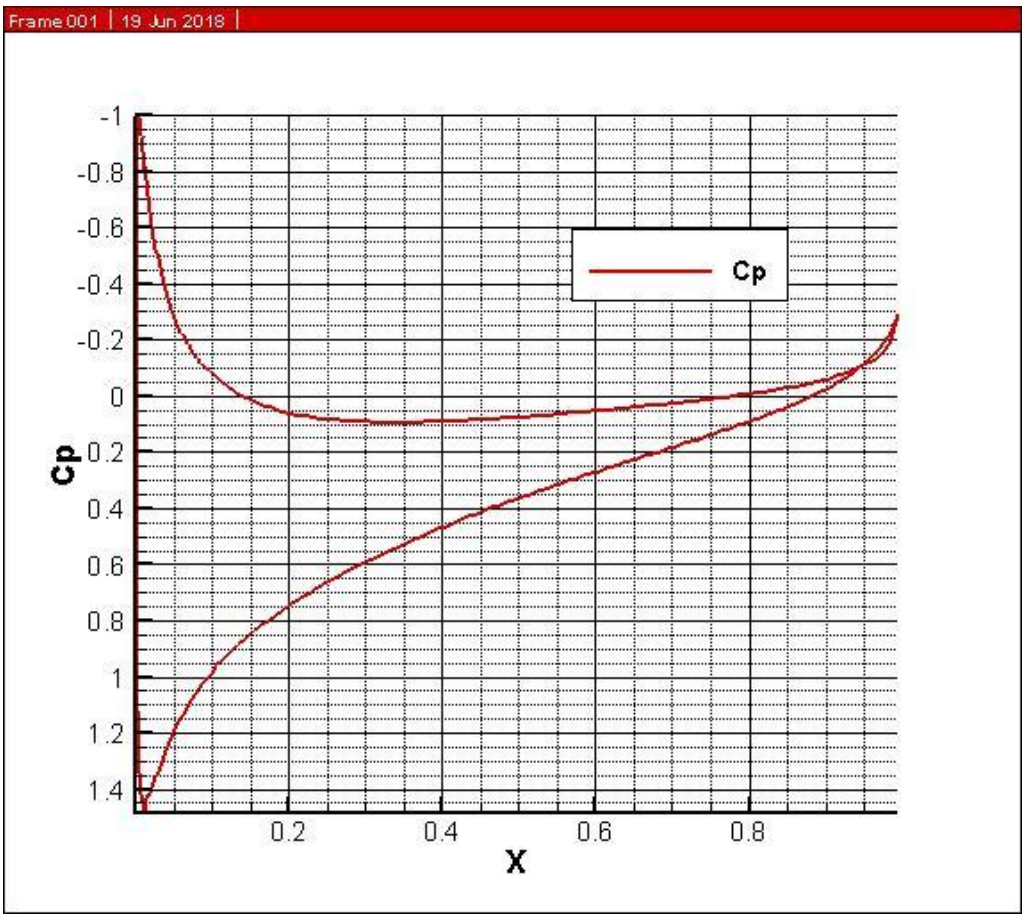

Figure 6-5. Pressure Coefficient of the NACA Profile.

In Figure 6-5, we can appreciate how the greater gradient of pressure is at the beginning of the surface. It starts at 0.05 approximatly until 0.4.

The next step is to change the number of stations to to obtain the greatest section for suction. This will be shown in the diagrams of the velocity component u versus η. The velocity for suction will be the same of a value of 0.1. The first try will be with suction starting before the case in Figure 6-1, so now the first station starts at 50 and the same ending of 180. The Figure 6-6 is for section 112 for the three cases exposed.

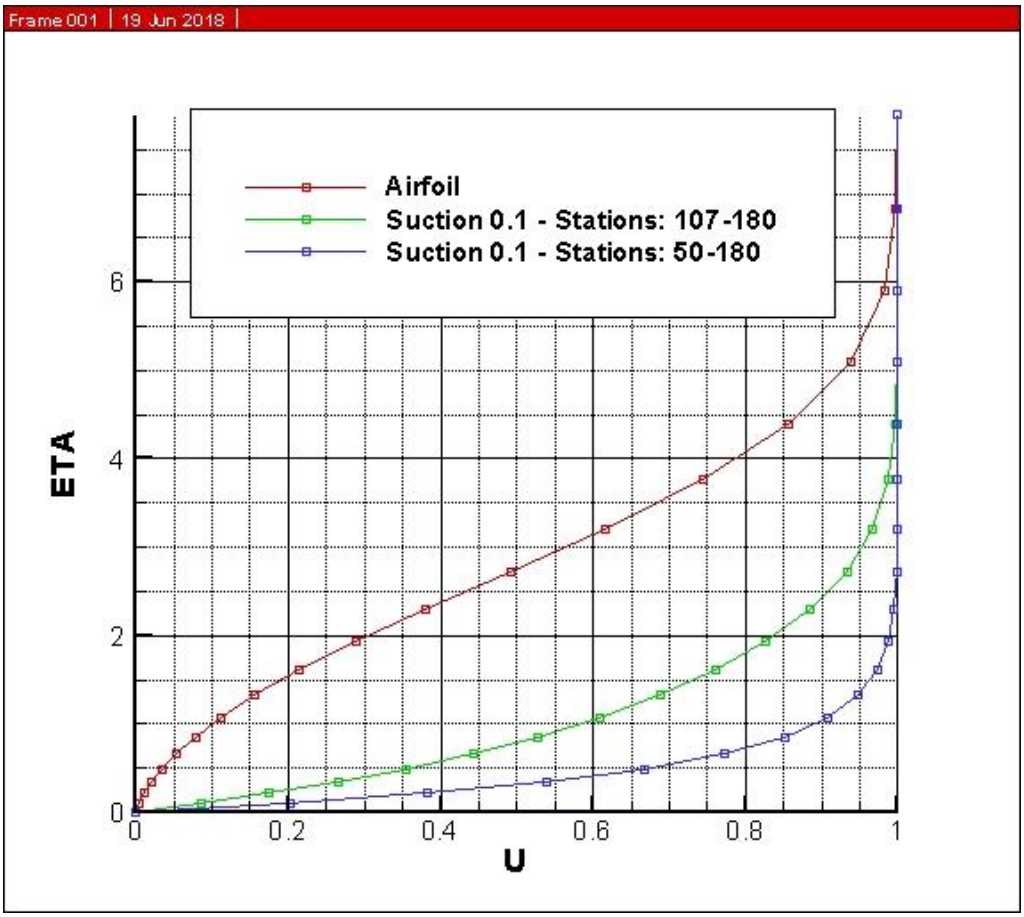

Figure 6-6. Comparison for station 112 between two different sections for suction effect.

In Figure 6-6 can be appreciated how the new section chosen produces a greater velocity profile for the same coordinates. So that, the effect of suction is more effective in this area rather than the one tried for the first case.

There have been other studies for different section range, but the best result is the one shown in Figure 6-6. For Section 6.3 the configuration chosen to find out the best value of the suction velocity will be the one between stations 50 until 180.

6.3 Value of v_w

To study the best value for suction and blowing velocity, we start changing the value by increasing it. For the case of suction, we already know the optimum section where the effect is more effective.

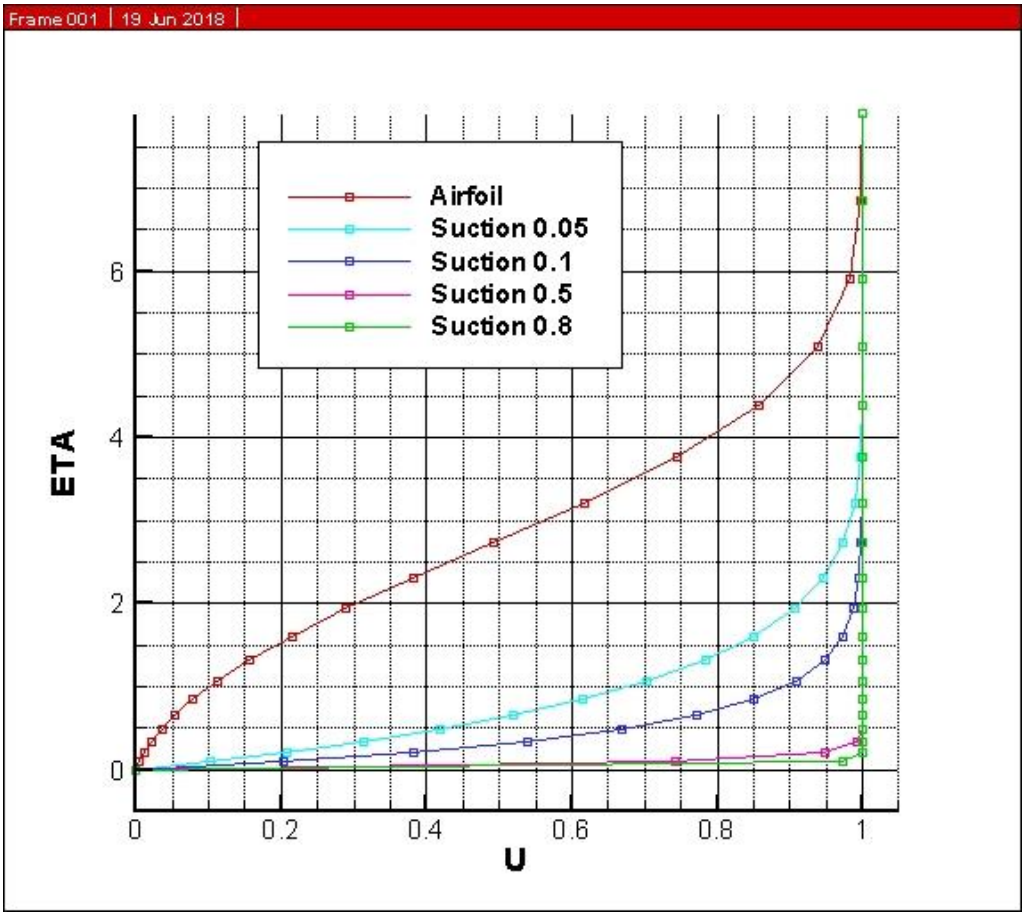

Figure 6-7. Comparison for different values of velocity suction for station 112.

In Figure 6-7 it is shown how we can still increasing the suction velocity, but as long as we keep increasing it we also obtain higher values for friction coefficient. In order to know the value that will provide a smaller friction coefficient, we need to compare the friction coefficient of the results for station 112.

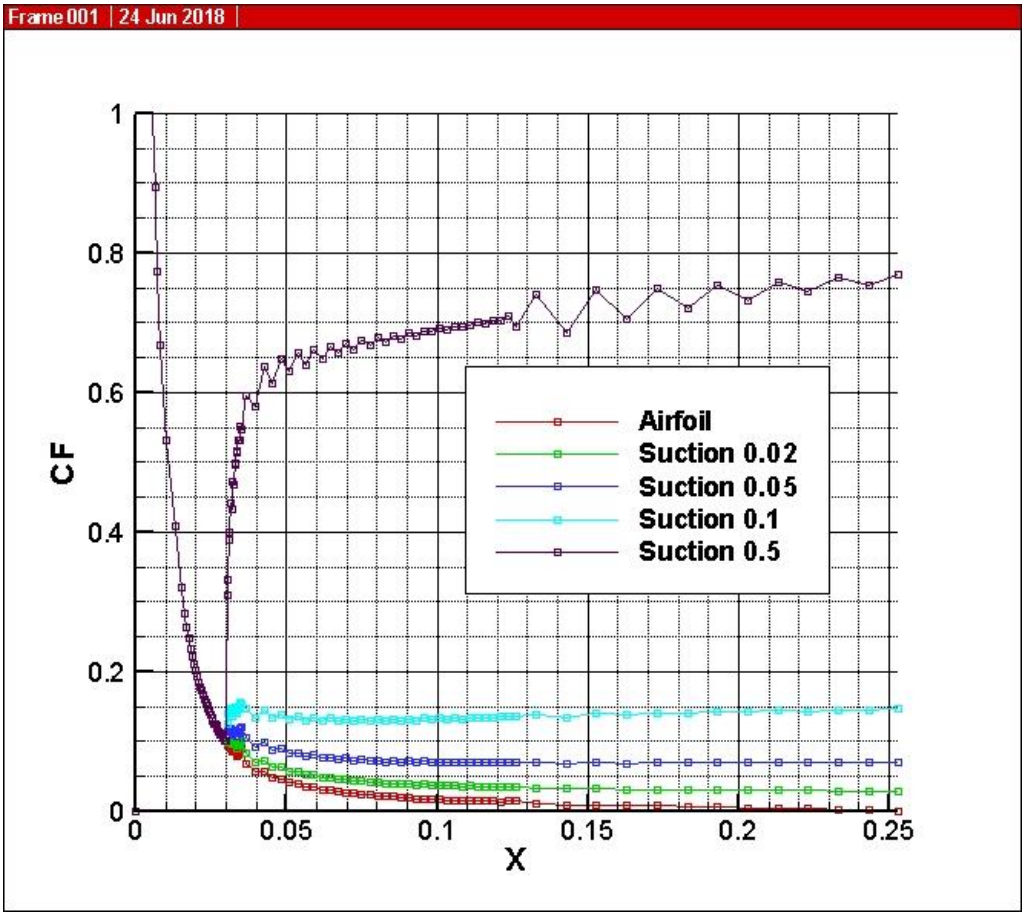

Figure 6-8. Comparison of the Ficrtion Coefficient.

Figure 6-8 shows how the best value for a smaller friction coefficient would be a velocity suction of -0.02 or -0.05 value. This will provide an increasement for the velocity component *u* of the boundary layer and a small value for friction.

6.4 Turbulent Flow and Blowing Effect

Blowing effect can be useful for turbulent flows, this is due to the turbulence present in the boundary layer. The injection of a flow in the upper surface of an airfoil produces a greater u^+ velocity as we can see in Figure 6-9. The other parameters of the boundary layer are studied and shown in the next subsections.

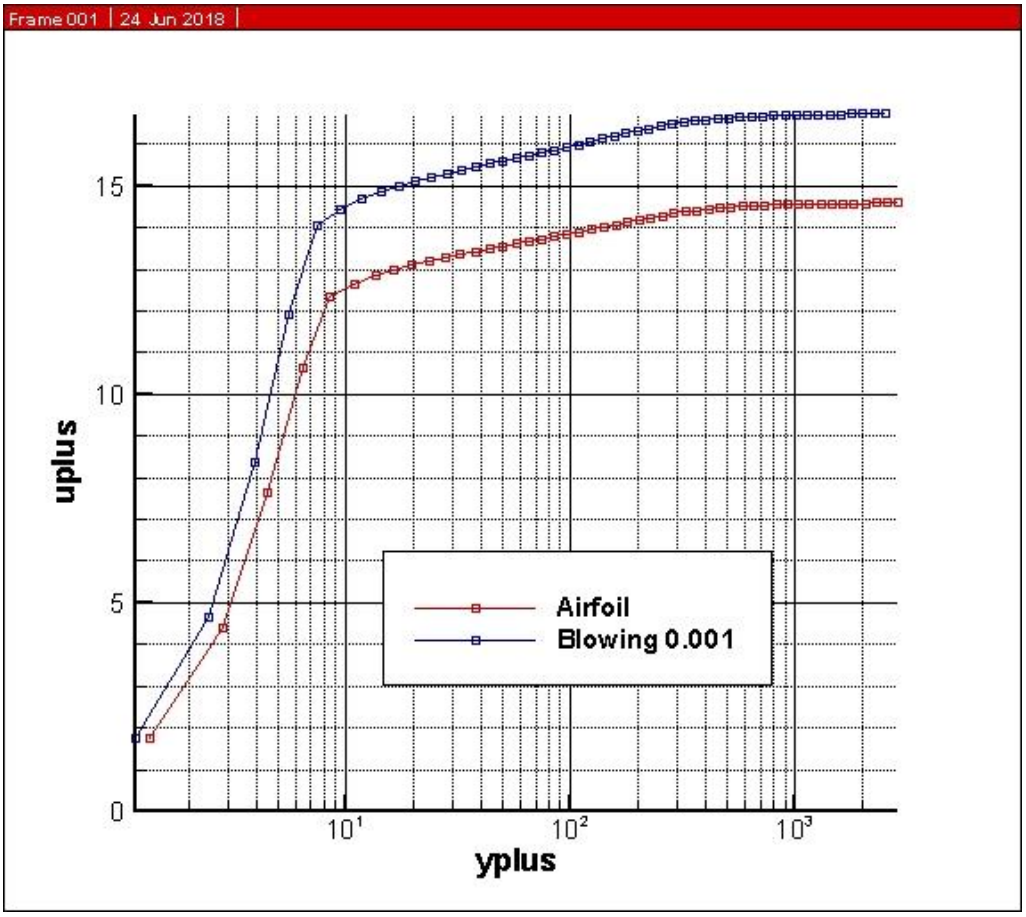

Figure 6-9. U+ vs Y+ for Blowing.

6.4.1 *Cf* vs *x*

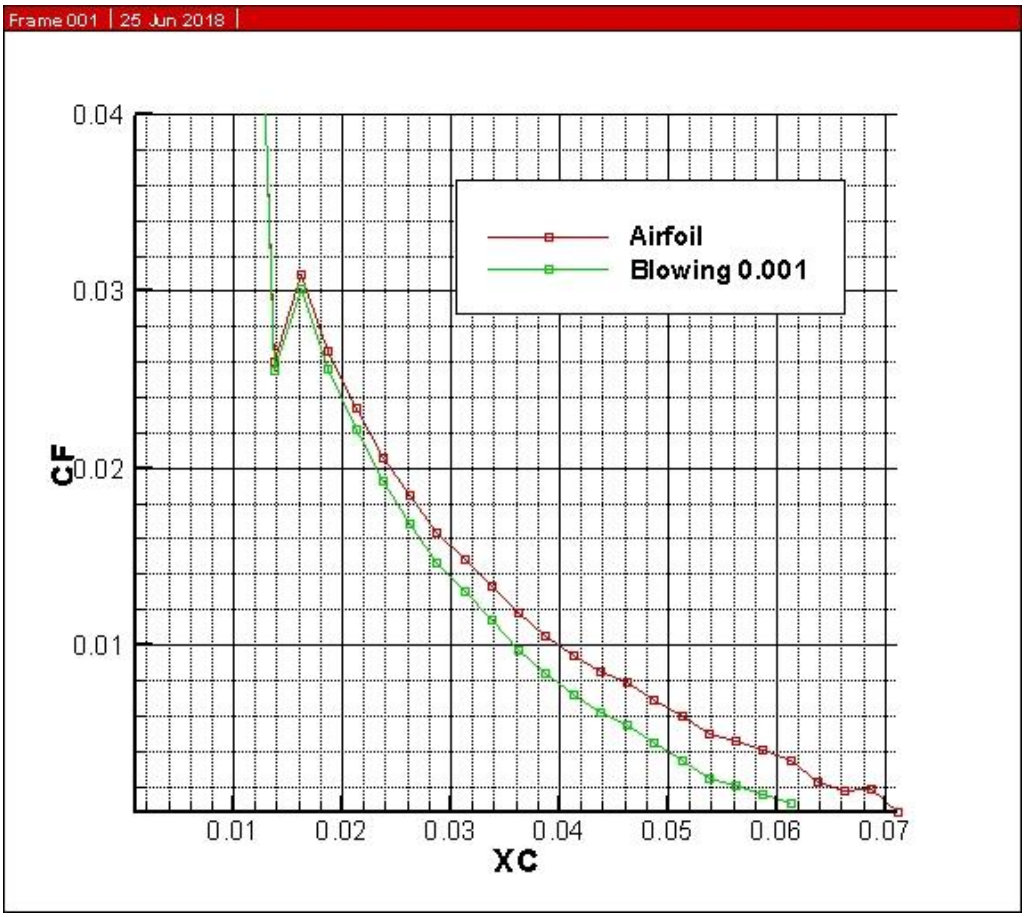

Figure 6-10. Friction coeffficient versus x for turbulent flow.

Figure 6-10 shows how the blowing effect benefits the boundary layer by decreasing the friction coefficient.

6.4.2 δ^* vs x

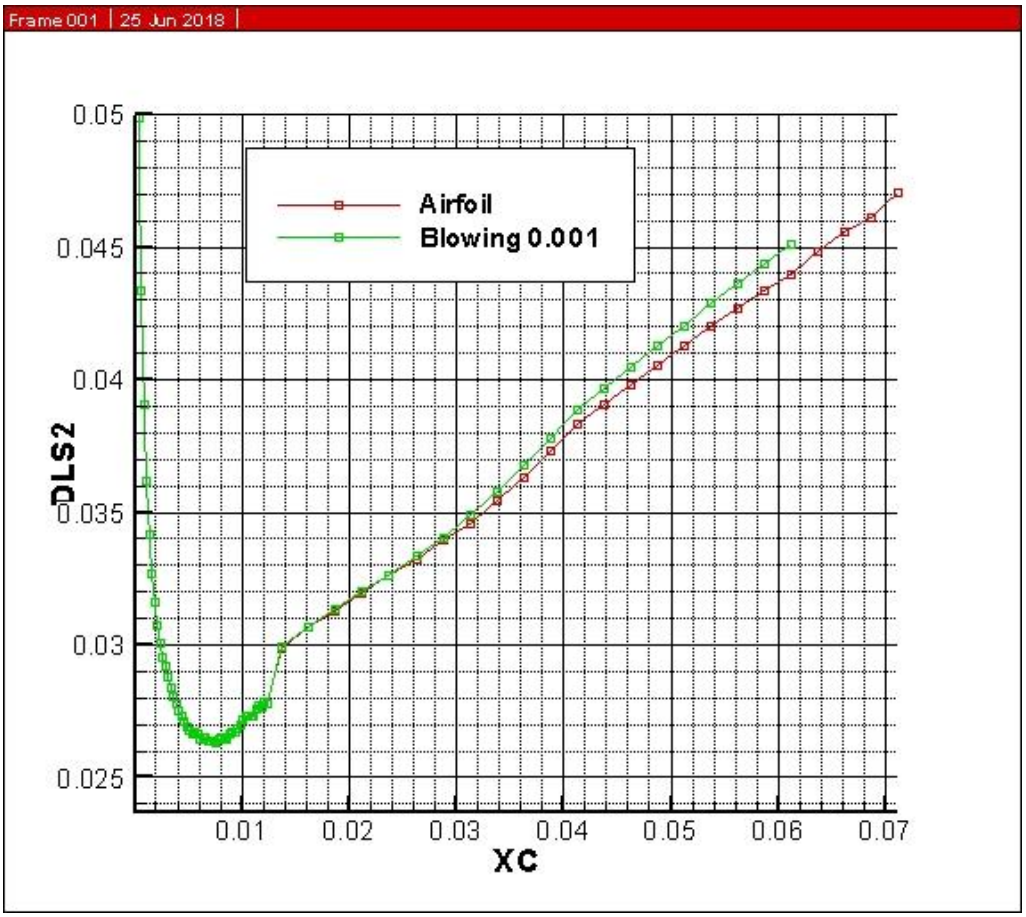

Figure 6-11. Displacement thickness versus x for turbulent flow.

In Figure 6-11, it is shown the displacement thickness for the turbulent flow and how it has smaller values for the blowing case. This case has more calculations than the airfoil, due to the re-attachmetn of the turbulent boundary layer.

6.4.3 θ vs x

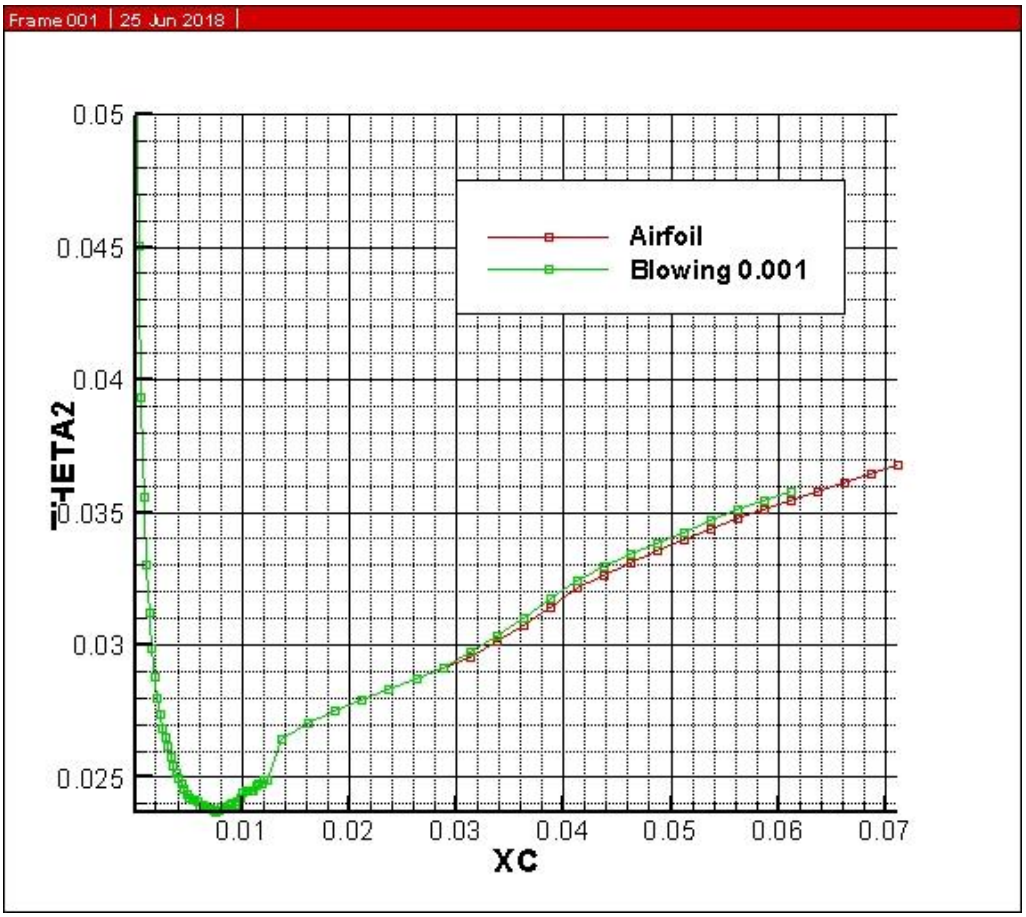

Figure 6-12. Theta versus x for turbulent flow.

In Figure 6-12 we can see how the momentum thicknes has similar values but smaller at the begginig of the station where the effect starts to take place. It is similar to the results shown before in Figure 6-11.

7 Conclusions

The boundary layer solution for the Blasius equation was a great achievement and still is very used nowadays. The simplest methods are useful to understand the complex problems and models. It also provides and approximation of the solution. The aim of this research is to keep researching about the boundary layer theory in order to determine as much information as possible of the boundary layer characteristics.

For the second part of the research, a deeper study has been carried out to calculate the main parameters of the boundary layer with the cases of suction and blowing. It has been proved how for laminar flows it is convenient to choose suction with a value around 0.02 and for stations starting at the begging of the surface until the end of the surface. This produces a re-attachment in the boundary layer delaying the separation from the body.

For turbulent flows it is useful to add a small velocity blowing at the surface in order to attach the turbulent flow in the upper surface. These results were obtained using a FORTRAN code provided from the books [2] and [3] and modifying some parts to add the blowing and suction effect.

To conclude, it has been proved how these two effects benefits the behavior of the boundary layer under the right conditions and it is an approach for researching in method of increasing the aerodynamic efficiency of the airfoil.

8 References

[1] Schlichting, H., Gersten, K., “Boundary layer theory”, Germany, Springer.
[2] Cebeci, T., Cousteix, J., “Modeling and Computation of Boundary-Layer Flows”, Springer.
[3] Cebeci, T., “Turbulence Models and Their Application”, Springer.
[4] Hazen. D., “Boundary Layer Control”, National Committee for Fluid Mechanics Films.